

TEL AVIV UNIVERSITY

The Iby and Aladar Fleischman Faculty of Engineering
The Zandman-Slaner School of Graduate Studies

**A MODEL OF CATERPILLAR
LOCOMOTION BASED ON ASSUR
TENSEGRITY STRUCTURES**

A thesis submitted toward the degree of
Master of Science in Mechanical Engineering

By
Omer Orki

May 2012

TEL AVIV UNIVERSITY

The Iby and Aladar Fleischman Faculty of Engineering
The Zandman-Slaner School of Graduate Studies

**A MODEL OF CATERPILLAR
LOCOMOTION BASED ON ASSUR
TENSEGRITY STRUCTURES**

A thesis submitted toward the degree of
Master of Science in Mechanical Engineering

By
Omer Orki

The research was carried out in the School of Mechanical Engineering
under the supervision of
Prof. Offer Shai
and Dr. Uri Ben-Hanan

May 2012

Acknowledgments

First and foremost I would like to thank god.

I am also grateful for my supervisors and the members of the research team for their help with this study:

Prof. Offer Shai

Dr. Uri Ben-Hanan

Prof. Amir Ayali

Dr. Efim Mohr

Mr. Michael Slavutin

Mr. Dima Mazor

I would also like to give special thanks to Mitchell Kennard who proofread the thesis.

Last but not least, I wish to thank my family, without whom none of this would have been possible.

Omer Orki.

Abstract

Caterpillars are soft-bodied animals and use fluid and tissue pressure to stiffen their body, a mechanism known as hydrostatic skeleton. They have a relatively simple nervous system, but are still able to perform a variety of complex movements.

This thesis presents a 2D caterpillar simulation which mimics caterpillar locomotion using Assur tensegrity structures. Tensegrity structures are structures composed of a discontinuous set of compressed components inside a continuum of tensioned components. Their stability is maintained by the self-equilibrated state of all elements. Assur tensegrities are a novel sub-group of tensegrity structures.

In the model, each caterpillar segment is represented by a 2D tensegrity triad consisting of two bars connected by two cables and a strut. The two cables represent the two major longitudinal muscles of the caterpillar, while the strut represents hydrostatic skeleton. In addition to the mechanical structure, the control scheme in this model is also inspired by the biological caterpillar.

The unique engineering properties of Assur tensegrity structures, together with the suggested control scheme, provide a model with simple and intuitive control. In addition, the model segments have a controllable degree of softness - each segment can be either soft or rigid.

The model also exhibits several characteristics which are analogous to those of the biological caterpillar. One such characteristic is that the internal pressure of the biological caterpillar is not a function of its size. During growth, body mass is increased 10,000-fold while internal pressure remains constant. In the same way, our model is able to use the same internal forces regardless of model size. Our research also suggests that caterpillars don't invest considerably more energy while crawling than while resting.

Table of Contents

1	Introduction.....	1
1.1	Previous work.....	2
1.2	Objective.....	4
1.3	Overview of thesis.....	4
2	Biological back ground.....	5
2.1	Caterpillar anatomy.....	5
2.2	Caterpillar locomotion.....	6
3	Tensegrity.....	8
3.1	Definition.....	8
3.2	Tensegrity in nature.....	9
3.3	Form finding.....	9
3.4	Infinitesimal mechanism.....	10
3.5	Stability.....	11
3.6	Shape change algorithms.....	11
4	Physical foundation underlying the model.....	14
4.1	Classification of trusses.....	14
4.2	Assur trusses.....	16
4.3	Assur tensegrity structures.....	17
4.4	Shape change of Assur tensegrity structures.....	18
5	Model basics.....	21
5.1	The mechanical model.....	21
5.1.1	The model segment.....	21
5.1.2	Legs.....	22
5.1.3	The complete model.....	22
5.2	Stability.....	23
5.2.1	The principle of potential energy.....	23
5.2.2	Analyzing triad stability.....	24
5.2.3	Additional triad configurations.....	28
5.3	Shape change.....	28

5.4	Softness.....	30
5.5	Chapter Summary.....	32
6	Model enhancements.....	33
6.1	Impedance control.....	33
6.1.1	Motivation for impedance control.....	34
6.1.2	Introduction to impedance control.....	36
6.1.3	Implementation of impedance control.....	37
6.1.4	Stability.....	38
6.1.5	Shape change.....	39
6.1.6	Softness.....	39
6.2	Area conservation.....	40
6.2.1	Nomenclature.....	40
6.2.2	Motivation for area conservation.....	41
6.2.3	Implementation of area conservation.....	42
6.2.4	Stability.....	43
6.3	Final segment model.....	44
6.3.1	Shape change.....	46
6.3.2	Softness.....	47
6.3.3	Determining the magnitude of the internal torque coefficient.....	49
7	Caterpillar Control.....	51
7.1	Control Scheme.....	51
7.2	Low-level control.....	53
7.2.1	Struts.....	53
7.2.2	Cables.....	53
7.2.3	Legs.....	55
7.3	High-Level Control.....	55
7.3.1	Level 1 control.....	57
7.3.2	Level 2 control.....	58
8	Results.....	62
8.1	Model Characteristics.....	62
8.2	Kinematic results.....	62
8.2.1	Crawling stages.....	62
8.2.2	Segment length.....	63

8.2.3	Crawling parameters	64
8.3	Cable dynamics	65
8.4	Different terrains	67
8.5	Other results.....	68
8.5.1	Area conservation.....	68
8.5.2	Internal Pressure	69
9	Discussion	70
9.1	Controlling Assur tensegrity structures using impedance control.....	70
9.2	Caterpillar model.....	71
9.3	Further Research.....	73
	Bibliography.....	74
	Appendix A - Development of the equations for shape change and softness.....	77
A.1.	Shape change without external forces	77
A.2.	Softness.....	78
A.2.1.	Axial force	78
A.2.2.	Bending torque	80
A.2.3.	Bending force	81
	Appendix B - Single-segment algorithm	83

List of Figures

Figure 1.1: The inchworm robot of Wang et al.	2
Figure 1.2: Stulce's model for a multibody legged robot.	2
Figure 1.3: Trimmer's soft robot.	3
Figure 1.4: A 15-bar tensegrity model built by Rieffel et al.	4
Figure 2.1: <i>Manduca sexta</i> anatomy.	5
Figure 2.2: Several caterpillar muscles.	6
Figure 2.3: The inchworm inching gate.	6
Figure 2.4: The crawling gate of <i>Manduca Sexta</i>	7
Figure 3.1: A few examples of tensegrity structures.	8
Figure 3.2: Four-bar mechanism with different bar lengths.	10
Figure 3.3: The infinitesimal mechanism of a dyad.	10
Figure 3.4: Stabilization of tensegrity structure	11
Figure 3.5: An equilibrium manifold.	12
Figure 4.1: A four bar mechanism.	14
Figure 4.2: Classification of static trusses.	15
Figure 4.3: An example of a topological exception	15
Figure 4.4: An example of a geometrical exception.	16
Figure 4.5: An example of an Assur and non-Assur truss	16
Figure 4.6: Decomposition of a determinate truss into Assur trusses.	17
Figure 4.7: The singular configuration of a triad	18
Figure 4.8: Special configurations of non-Assur determinate trusses	18
Figure 4.9: Singular configuration	19
Figure 4.10: The experimental robot.	20
Figure 5.1: The model triad as compared to the standard triad.	21
Figure 5.2: The caterpillar model.	23
Figure 5.3: Two options for tensegrity triad configuration.	24
Figure 5.4: Stability analysis – case 1	25
Figure 5.5: Velocity diagram of the triad.	25

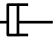
Figure 5.6: Velocity and radial acceleration of point C.	26
Figure 5.7: Acceleration diagram– case 1	26
Figure 5.8: Stability analysis – case 2.....	27
Figure 5.9: Acceleration diagram– case 2.....	27
Figure 5.10: Two additional triad configurations.	28
Figure 5.11: Nomenclature for the inverse kinematics calculation.	29
Figure 5.12: The effect of external forces on the triad shape.	31
Figure 5.13: The change of the triad shape due to external force	32
Figure 6.1: Triads between two walls.	33
Figure 6.2: Illustration of the shortcoming of the basic control algorithm	34
Figure 6.3: Two force-controlled elements.....	35
Figure 6.4: Potential energy graph. Two cables under constant force control.	35
Figure 6.5: Potential energy graph. Two cables under impedance control.....	38
Figure 6.6: Describing a frame in plane.....	40
Figure 6.7: Segments subjected to pure bending and pure shear	41
Figure 6.8: The model is too sensitive to shear movement.....	41
Figure 6.9 : Segment area in pure shear.....	42
Figure 6.10: Internal torque.	42
Figure 6.11: The effect of internal torque.	43
Figure 6.12: Potential energy graph. Impedance control and internal torque.....	44
Figure 6.13: Final segment model	45
Figure 6.14: Segment lengths, forces, torques and reactions.....	46
Figure 6.15: Three cases of external load	47
Figure 6.16: A grounded segment has only one DOF.	49
Figure 6.17: The problem of high c when several segments are grounded.	49
Figure 6.18: Using a c that enables a small shear angle.	50
Figure 7.1: Hierarchy of the control scheme.....	52
Figure 7.2: Experimental data for loading–unloading response	53
Figure 7.3: The cable controller	54
Figure 7.4: Leg locking algorithm.	55
Figure 7.5: Numbering of the legs, cables and segments.	56
Figure 7.6: A complete stride of the caterpillar model	56
Figure 7.7: The commands sent to the cables and legs in step 1.	58

Figure 7.8: Illustration of the two-segments algorithm.	59
Figure 7.9: Calculating the output commands of level 2 control.....	61
Figure 8.1: Crawl Stages.	63
Figure 8.2: Strut length during crawling.	64
Figure 8.3: Movement of the center of mass during crawl.....	65
Figure 8.4: Force development under a tetanic stimulus	66
Figure 8.5: The change of cable force in <i>H3</i>	66
Figure 8.6: Model climb of sharp incline.....	67
Figure 8.7: Model climb through curved terrain.....	67
Figure 8.8: Model climbs upside down.....	68
Figure 8.9: Change in caterpillar area during crawling.	68
Figure 9.1: Comparing Assur tensegrity structures with other types of robots.	71
Figure A.1: Segment lengths, forces, torques and reactions	77
Figure A.2: A segment under axial force	78
Figure A.3: A segment under bending torque.....	80
Figure A.4: A segment under bending force.....	81
Figure B.1: The forces acting on each bar of a grounded segment.....	83
Figure B.2: The geometric parameters of the segment	83

List of Tables

Table 5.1: Comparison between caterpillar model and biological caterpillar.	23
Table 8.1: Strut length and step times during crawling.	64
Table 8.2: Time of force development under a tetanic stimulus at resting length.	66

List of Symbols

A, B, C	– Points
A_x, A_y	– Point elements
$\{A\}, \{B\}, \{C\}$	– Frames
F	– Internal force
F_0	– Virtual force
F_e	– External force
M_e	– External torque
M_i	– Internal torque
P	– Strut compression force
R	– Reaction
S	– Area
T_1	– Top cable tension force
T_2	– Bottom cable tension force
U	– Potential energy
a	– Acceleration
b	– Damping coefficient
c	– Internal torque coefficient
h	– Bar length
k	– Stiffness coefficient
l_0	– Virtual length
l_1	– Top cable length
l_2	– Bottom cable length
l_f	– Final length
l_i	– Initial length
l_s	– Strut length
v	– Velocity
φ_b	– Bending angle
φ_s	– Shear angle
ω	– Rotational velocity
-----	– Cable
—  —	– Strut

1 Introduction

The movement of animals with stiff articulated skeletons, such as vertebrates, tends to be fast and precise, using joints with a few degrees of freedom and relatively predictable limb kinematics. Often, only one or two muscles are needed in any particular movement. However, most living animals are soft-bodied and do not have hard skeletons. Instead they use fluid and tissue pressure to stiffen their body, allowing muscles to do useful work. This kind of mechanism is called a *hydrostatic skeleton*. As a result, the contraction of any one muscle affects all the rest, altering either their length or their tension [1].

Of these soft-bodied animals, caterpillars are particularly intriguing because they are very successful climbers that grasp and navigate in a complex three-dimensional environment. Their crawl is distinct from other soft-bodied animals like worms and molluscs. Caterpillars use passive grip to secure themselves to complex terrain and are able to bend, twist and crumple in ways that are not possible with a rigid skeleton. They use hydrostatics to vary body tension and can cantilever over gaps that are 90% the length of their body [2].

Most flexible biologically inspired robots are built from concatenated rigid modules with multi-axis joints between them. However, soft-bodied animals have no rigid skeleton at all. On the other hand, there have been few attempts to build completely soft robots (built from soft materials). However, these robots possess near-infinite degrees of freedom and have very complex dynamics which brings with it considerable complexity in control design [3].

This thesis presents a novel approach for simulation of the soft-bodied caterpillar crawl. The model is constructed from type of structures called *Assur tensegrity structures* (described in detail in chapter 4). The special properties of these structures together with the suggested control algorithm give the structure the ability to deform in response to external forces, a quality termed as *structural softness*.

1.1 Previous work

Several attempts have been made to build or simulate robots that mimic or are at least inspired by the caterpillar crawl.

Wang et al. [4] built two prototypes of a caterpillar robot. One employs inching gait (Figure 1.1), and the other employs crawling gait (explained in section 2.2). The robots are assembled using two types of modules: joint actuation modules and adhesion modules. The actuation module is driven by an embedded servo motor, while the adhesion module is equipped with a sucker and a releasing mechanism driven by a solenoid.

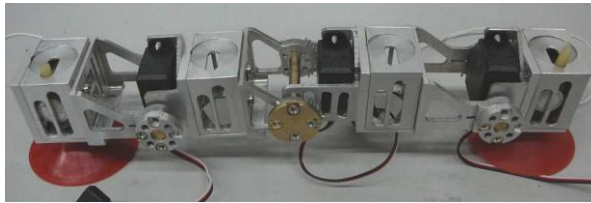


Figure 1.1: The inchworm robot of Wang et al.

Another model was introduced by Stulce [5]. He developed a computer simulation of a multibody robot with passive legs attached to it (a pair of legs for each body) based on observation of caterpillar specimen geometry, gaits and leg trajectories. The robot was assembled using a series of actuated Stewart-platforms (parallel manipulators with 6 linear actuators) connecting the bodies as shown in Figure 1.2. At the basic level of control, Stulce used position control for all actuators. Therefore, even for the simplest motion, where only one pair of legs is lifted, the robot needs to coordinate accurate trajectories for each of the 12 actuators (6 on each side of the legs). He also uses "vision" techniques to generate terrain mapping for planning and generating global and local robot paths.

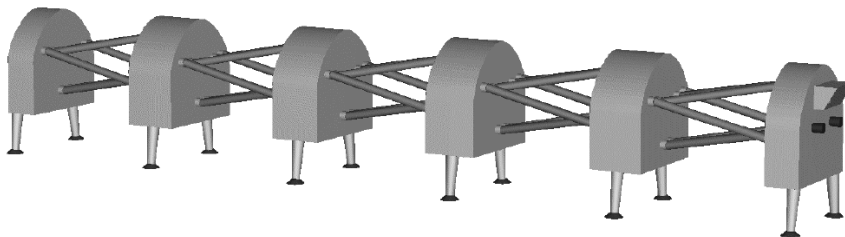


Figure 1.2: Stulce's model for a multibody legged robot.

In both cases, the caterpillar segments are modeled with rigid elements, in contrast with a biological caterpillar.

Trimmer et al. [3] developed a caterpillar model using soft and deformable materials. The main body of the robot is cast from a soft silicone elastomer and actuated using shape-memory alloy (SMA) wires. Their aim was to mimic the placement of muscles within the caterpillar model (Figure 1.3a).

However, the immense gain in flexibility and deformability brings with it considerable control complexity. Soft-bodied robots can possess near-infinite degrees of freedom. As a result, conventional methods of robotic control (used with considerable success in rigid, jointed mechanical systems) no longer apply.

To compensate, they developed suitably realistic simulations of the soft-bodied robot and tried to use genetic algorithm methods to discover control schemes [6] (Figure 1.3b). The authors did not report results in their paper and indicated that they still have much work to do.

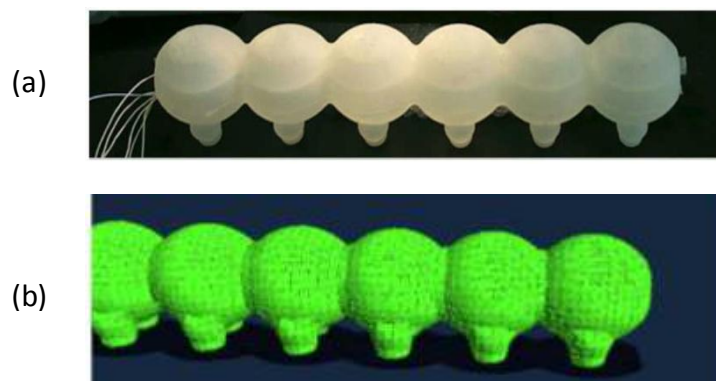


Figure 1.3: Trimmer's soft robot: (a) the physical soft robot, and (b) the corresponding simulation model.

Rieffel et al. [7] built a 15-bar, highly indeterminate tensegrity model, inspired by the caterpillar structure as shown in Figure 1.4. The high degree of dynamic coupling and complexity renders it largely unsuitable for control through conventional means. Instead, they used a variant of the artificial neural networks (ANNs) method called spiking neural networks (SNNs). The result is locomotion which is neither inspired by nor resembles the caterpillar crawl. Also, only the cables are actuated in this model. Struts are rigid bodies and remain at the same length. As a result, the model has a limited ability to change shape.

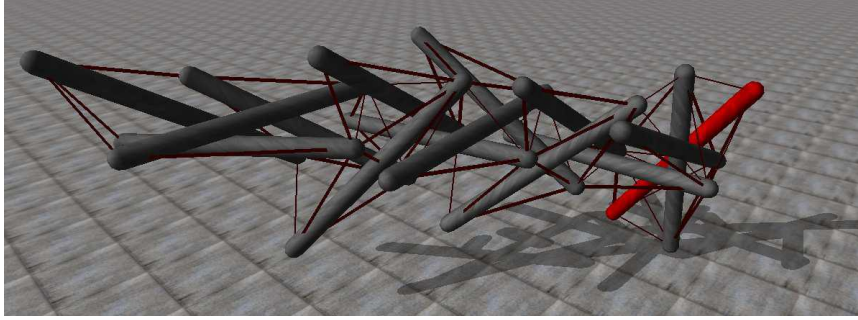


Figure 1.4: A 15-bar tensegrity model built by Rieffel et al.

1.2 Objective

The aim of this thesis is to simulate soft-bodied caterpillar crawl using Assur tensegrity structures. The Assur structure that was chosen to represent the caterpillar segment is a triad. The shape change algorithm that was used as the basis for my work is described in section 4.4.

Note the design of the model was primarily inspired by biological behavior and less by mechanical design feasibility; the model does not offer detailed mechanical specifications but rather represents a conceptual breakthrough.

1.3 Overview of thesis

Chapters 2-4 present the theoretical background of our work: Chapter 2 gives a biological background on caterpillars. Chapter 3 gives a review of tensegrity structures and the main properties and concepts of these structures. Chapter 4 introduces a family of determinate topologies called Assur trusses and presents some of its unique geometric properties. It then provides details concerning a sub-group of tensegrity structures called Assur tensegrity structures, and described a shape change algorithm for these structures.

Chapters 5-7 describe the caterpillar model: Chapter 5 introduces the three main characteristics of the model: stability, shape change and softness. Chapter 6 further develops those concepts and describes the final model. The full control algorithm is described in chapter 7.

Chapter 8 is the results chapter. Discussion and further research suggestions are presented in chapter 9.

2 Biological background

2.1 Caterpillar anatomy

Most of the biological research regarding caterpillars was done on the *Manduca Sexta* caterpillar (also known as the tobacco hornworm). As with all insects, its body is divided into the head, thorax and abdomen. The thorax consists of three segments, each bearing a pair of true, articulated legs. The abdomen, which constitutes over three quarters of the total caterpillar length, has eight segments – abdominal segments A1-A7 and the terminal segment TS. Abdominal segments three to six (A3-A6) and the terminal segment (TS) have fleshy protuberances called prolegs (Figure 2.1). The prolegs grip the surface passively and can be actively released and retracted.

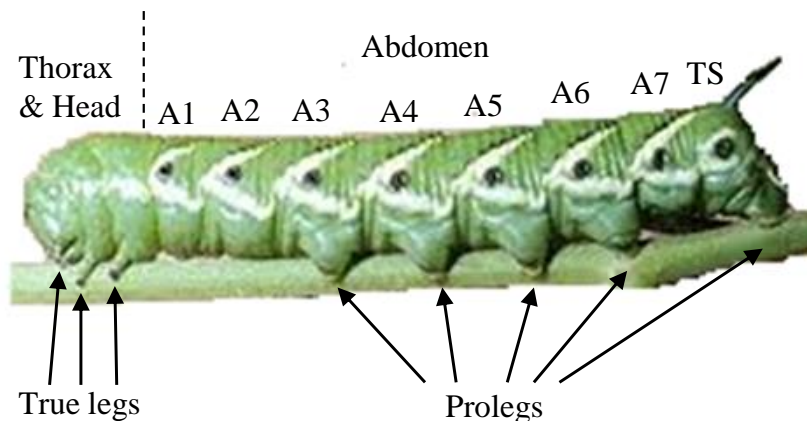


Figure 2.1: *Manduca sexta* anatomy.

Muscles are attached to the inside surface of the body wall. The musculature is complex. Each abdominal body segment contains around 70 discrete muscles (each having unique attachment points)! Caterpillars do not have circular muscles as do worms.

The major abdominal muscles in each segment are the ventral longitudinal muscle (VL1) and the dorsal longitudinal muscle (DL1) shown in Figure 2.2. Note that the VL1 is not a single muscle that extends the entire length of the caterpillar body. Each segment has its own distinct VL1 muscle which is controlled separately from the

others. The same is true for the DL1 muscle (and virtually all other caterpillar muscles). Each VL1 and DL1 muscle is attached to the sternal and tergal antecosta respectively (the antecostae are stiff ridges formed at the primary segmental line and provide a surface for the attachment of muscles) [8].

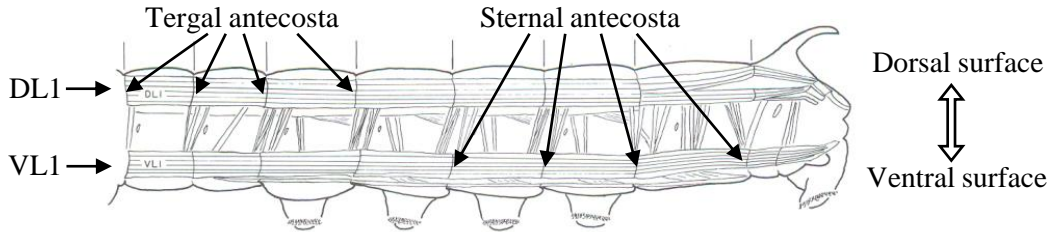


Figure 2.2: Several caterpillar muscles including the ventral longitudinal muscle (VL1) and the dorsal longitudinal muscle (DL1).

Caterpillars have a relatively simple nervous system, each segment having a ganglion (a nerve complex) which monitors movements. Despite their limited control resources, caterpillars are still able to coordinate hundreds of muscles in order to perform a variety of complex movements. It has been argued [9] that the mechanical properties of the muscles are responsible for some of the control tasks that would otherwise be carried out by neural control. It is also assumed that some muscles function primarily to maintain turgor, whereas others are primarily locomotory.

2.2 Caterpillar locomotion

There are two types of caterpillar locomotion. The first type is the inching gait of the inchworm (despite its name, the inchworm is a caterpillar and not a worm) shown in Figure 2.3.

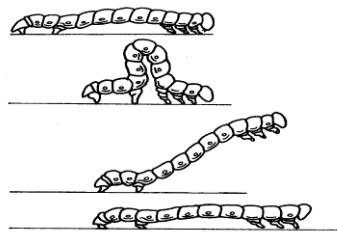


Figure 2.3: The inchworm inching gait.

The second type of locomotion is the crawling gait used by the *Manduca Sexta* and many other species. Crawling gait is the locomotion strategy used in this thesis. In

crawling gait, caterpillars crawl via a wave of muscular contractions that starts at the posterior and progresses forward to the anterior (note that throughout this thesis, the words “posterior” and “anterior” will be used to describe the anatomical directions as shown in Figure 2.4) [2]. This motion may reflect the output of a Central Pattern Generator (CPG), which is a neural mechanism that produces rhythmic patterned outputs [10].

During motion, at least three segments are in varying states of contraction at any given time. This is done to increase the length of a stride. The two legs on either side of each body segment move together as a unit.¹ Stride frequency is the dominant mechanism for controlling speed. As speed increases stride frequency can increase by a factor of four.

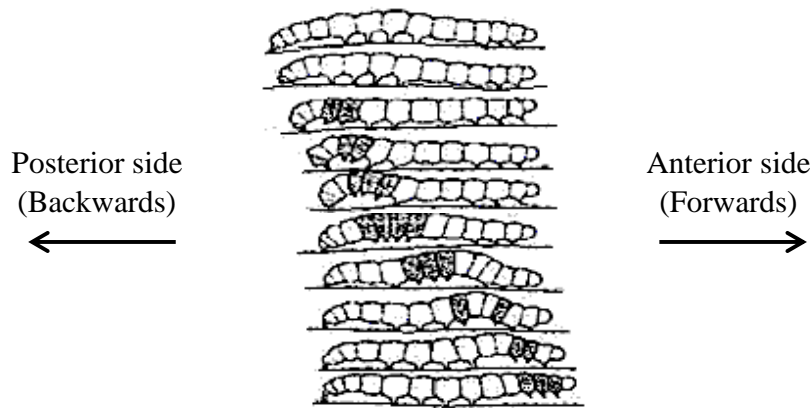


Figure 2.4: The crawling gait of *Manduca Sexta*.

Caterpillars do not use the prolegs as actuated propulsive limbs; instead, they use them as support and to generate controllable grip of the terrain. Prolegs have powerful passive attachment to the terrain. Once a particular proleg pair has moved and “planted”, there is no further movement by that proleg or body segment until the next stride.

Use of a hydraulic mechanism for terrestrial locomotion (as in the case of caterpillar locomotion) is considerably more energy expensive than use of muscles attached to a rigid skeleton. The explanation for this higher cost of transport appears to rest in biomechanics rather than in muscle performance [11].

¹ This in-phase motion of the two legs is very unusual in insects. With most other insects the two legs of each segment move exactly a half-cycle out of phase from each other.

3 Tensegrity

3.1 Definition

The word Tensegrity is a contraction of ‘tensional integrity’ which was coined by Richard Buckminster Fuller [12].

It is difficult to precisely define tensegrity. Fuller described the tensegrity principle as “islands of compression inside an ocean of tension.” This broad definition of tensegrity would include a balloon: the air inside the balloon is under compression and the balloon envelope is under tension. Together, they form a stable system.

The “classic” tensegrity structure is a truss-like structure that is composed of struts² under compression and cables under tension. A more strict definition for these tensegrity systems was given by Motro: “A tensegrity system is a system in a stable self-equilibrated state comprising a discontinuous set of compressed components inside a continuum of tensioned components” [13]. Several examples of this kind of tensegrity system can be found in Figure 3.1.

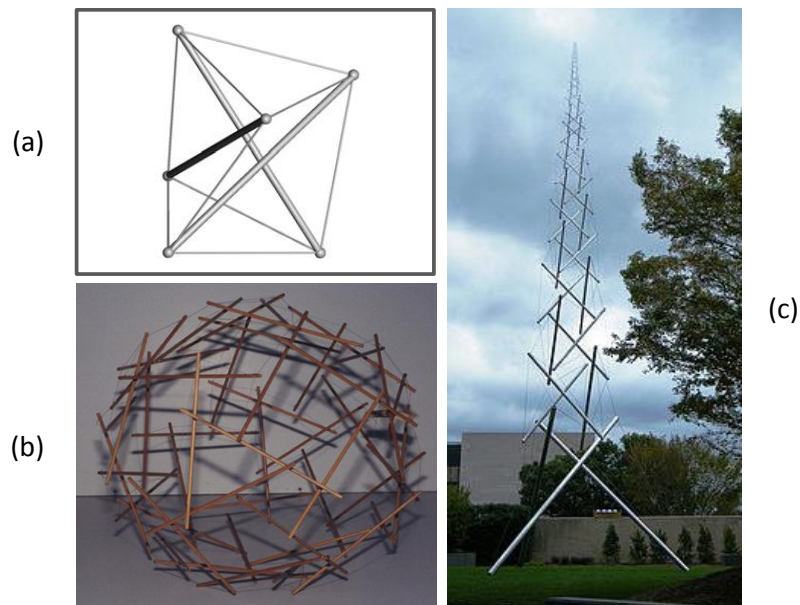


Figure 3.1: A few examples of tensegrity structures: (a) the simplest spatial tensegrity structure, also known as a “simplex”, (b) the original Fuller tensegrity in the Stanford archive, and (c) Snelson's needle tower.

² In tensegrity terminology the bars in compression are called struts.

3.2 Tensegrity in nature

Principles of tensegrity can be found at essentially every scale in nature. At the macroscopic level, the 206 bones that constitute the human skeleton are upheld against the force of gravity and stabilized in a vertical form by the pull of tensile muscles, tendons and ligaments. At the cellular level the cytoskeleton (the cell's internal skeleton) consists of three major components: microfilaments, microtubules and intermediate filaments. A gossamer network of contractile microfilaments extends throughout the cell, exerting tension. Opposing this inward pull are the microtubules, exerting compression. The intermediate filaments connect microtubules and contractile microfilaments to one another. At the other end of the scale, proteins and other key molecules in the body also stabilize themselves through the principles of tensegrity [17].

3.3 Form finding

Merely examining the topology of a tensegrity structure is not sufficient to determine whether it is rigid or not (as is the case for trusses). Even if the structure topology is suitable for a tensegrity structure, it will be rigid only in specific configurations. There is a fundamental question we have to answer when investigating tensegrity structures: under what conditions does a tensegrity structure yield rigidity with all cables in tension and all struts in compression? This problem is commonly referred to as the *form finding* problem.

A large number of truss topologies can move into special configurations in which they become tensegrity structures. These configurations correspond to specific link lengths of the system members which place the structure in a configuration called a *singular configuration*. Only in these singular configurations will the structure not collapse when specified rigid links are replaced by flexible tension members. These tensegrity configurations allow the system to be self-stressed, which a tensegrity system requires to obtain stiffness. For example, to build a regular³ simplex, as shown in Figure 3.1a, the ratio between the length of the struts and that of the cables needs to be 1.468. A different choice for these values creates either a system without rigidity (if the ratio is too small) or a system which will be very difficult and perhaps even impossible to assemble (if the ratio is too large).

³ Regular tensegrity structures are structures in which all cables are of equal length and all struts are of equal length.

There are several methods for form finding. An example of a form finding method that uses a geometric approach was developed by Whittier [14]. This method is based on finding the *boundary of non-assembly*. The method employs the fact that in any structure or mechanism a set of link lengths can be found that does not allow the system to be assembled. Bar systems can also be constructed of link lengths such that they exist on the boundary of non-assembly. An example of this is shown in Figure 3.2. The theorem of Whittier says that tensegrity configurations lie on the boundary of non-assembly for trusses and mechanisms.

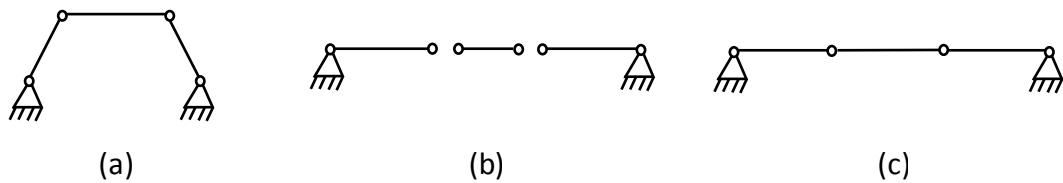


Figure 3.2: Four-bar mechanism with different bar lengths. In Mechanism (a) the chosen set of link lengths allows assembly. The links of Mechanism (b), on the other hand, have been chosen such that the mechanism cannot be assembled. Mechanism (c) has been built so that it is on the boundary of non-assembly.

3.4 Infinitesimal mechanism

Along with the ability of having self-stress (sometimes also referred as pre-stress), all tensegrity structures have infinitesimal flex from an infinitesimal mechanism. The infinitesimal mechanism is the ability of the structure to move in a certain direction an infinitesimal amount without extending (or contracting) the length of any of the links. A simple example of this infinitesimal mechanism can be seen in the two dimensional structures (called dyads) shown in Figure 3.3. If a vertical displacement is applied to the center node of the dyad, there is nothing to resist the initial displacement. That initial displacement is the infinitesimal mechanism. As the mechanism attempts to displace a finite amount, the displacement will be resisted by the required lengthening of the members that removes this degree of freedom.

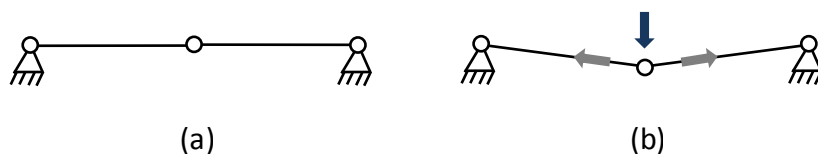


Figure 3.3: The infinitesimal mechanism of a dyad.

3.5 Stability

Let us consider the 2-bar dyad shown in the previous figure. The dyad can turn into a tensegrity structure by introducing self-stress. The self-stress can be added in the form of tension forces or compression forces. When tension forces are applied, bars are replaced with cables. When compression forces are added, the bars become struts.⁴ In both cases the system is in equilibrium state, but only one case is a stable equilibrium.

In the first case, if the junction node is taken away from its equilibrium location, the effect of the self-stress of tension returns it to the equilibrium location once the disruption is removed; the infinitesimal mechanism is stabilized by the tension self-stress (Figure 3.4a). In the opposite case, the system will not return to its equilibrium location; the system was in an unstable equilibrium (Figure 3.4b). Only the first case is a tensegrity system.

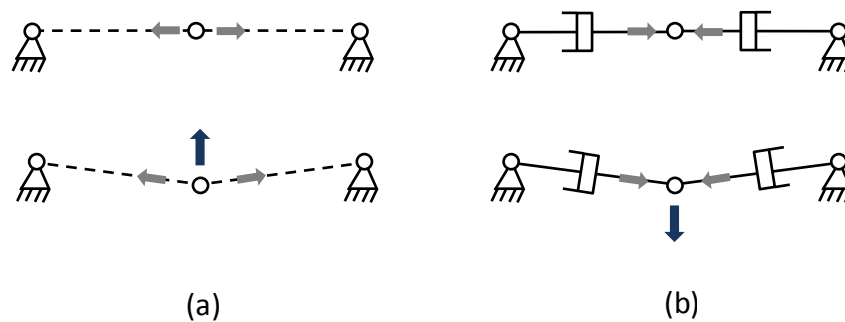


Figure 3.4: Stabilization of tensegrity structure: (a) a stable dyad composed of two cables in tension, and (b) an unstable dyad composed of two struts in compression.

3.6 Shape change algorithms

Although tensegrity structures are, by definition, static structures, they can be made into robots that can change shape. Shape change is a process in which, by adjusting the length of some of tensegrity structure members, the geometry of the structure is altered.

Note that the motion must be made while maintaining structural stiffness. In other words, during motion the self-stress forces must be maintained.

Sultan and Skelton [15] presented a shape change strategy based on the identification of an *equilibrium manifold*, to which the initial and final configurations belong. The

⁴ Basically, struts are bars. The word “strut” is used to indicate that it is a compressed element.

equilibrium manifold is a set of points corresponding to stable tensegrity configurations (also known as equilibrium configurations). The idea is to conduct motion such that the motion path passes through the manifold points. The advantage in doing so is that the successive configurations that the structure passes through are not much different from the equilibrium ones.

Their paper presents a 2-stage 6-bar tensegrity robot (Figure 3.5a) that moves only in a particular set of symmetrical configurations. In this kind of motion, only three parameters are needed to describe the robot's position.

Due to the small number of parameters, the allowable configurations of the tensegrity structure can be conveniently visualized as an equilibrium surface plotted on a three dimensional graph, as shown in Figure 3.5b. Each dot on the graph represents an allowable equilibrium configuration that has been identified, and the black line represents the desired shape change path.

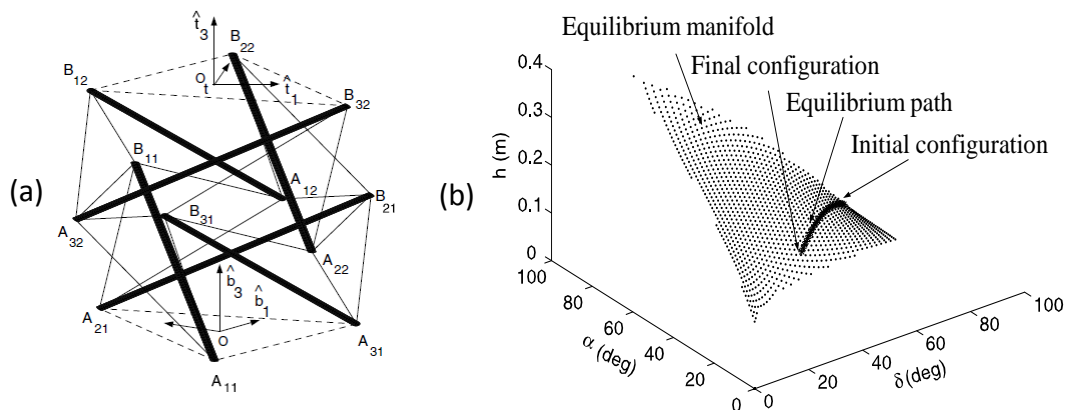


Figure 3.5: (a) A two-stage six-bar tensegrity structure; (b) an equilibrium manifold of the symmetrical configurations (the black line represents the shape change path).

This strategy is useful for such a symmetrical shape change where there are a small number of parameters. The problem is that there is a rapid increase in the number of independent parameters when asymmetrical shapes are considered. In those cases, the equilibrium manifold becomes too large, and a search to characterize this space would most likely be fruitless.

Van de Wijdeven and de Jager [16] developed a shape change algorithm by using an optimization method. In this algorithm the desired shape change and time span are divided into N sub-shape changes and time steps. The nodal positions of the tensegrity

structure are found at every sub-shape by solving a constrained optimization problem. Due to the number of nodes in a non-trivial structure, the optimization is of larger scale and it is also non-convex and nonlinear.

In both methods described above, motion is divided into many steps. For each step a form finding procedure is required (by predefined values or by an optimization method) and a path passing through all points must be calculated.

The algorithm presented in our work was developed using another, much simpler algorithm. This algorithm will be described in section 4.4.

4 Physical foundation underlying the model

The following chapter presents a different method for finding and analyzing tensegrity structures using Assur trusses. This chapter introduces the concept of Assur trusses and their unique engineering properties. It then explains how these structures can be made into tensegrity structures. Finally a new shape change algorithm is presented.

4.1 Classification of trusses

Engineering systems can be generally categorized into three groups: over-constrained, well-constrained and under-constrained. In CAD systems, for example, when too many dimensions are provided, the model is over-constrained because of redundancy. If insufficient dimensions are provided, the model cannot be produced and is under-constrained. Only when the minimum dimensions required to produce the model are provided is a system well-constrained.

The same categorization can be similarly applied to mechanical systems, including structures, mechanisms, robots, etc. Suppose we have a 2D truss with number of internal joints j (excluding ground joints). If the number of bars is less than $2j$, the structure would be under-constrained. These systems cannot sustain external force and are thus mobile. Figure 4.1 shows a system with 3 bars and 2 joints, which according to the above rule is mobile (a four-bar mechanism).

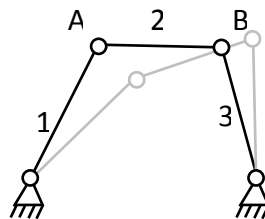


Figure 4.1: A four bar mechanism.

If the number of bars is exactly $2j$, the structure becomes rigid. This kind of structure usually cannot sustain self-stress forces when there is no external force applied to it. When there is an external force, it is possible to calculate all the forces on all the bars

using only force equilibrium around each joint. This is a well-constrained system, and it is known as a statically determinate truss (Figure 4.2a). When the number of bars exceeds $2j$, there is redundancy and the analysis is much more complicated, requiring consideration of additional parameters such as the material of the bars. This type of system is known as a statically indeterminate truss (Figure 4.2b).

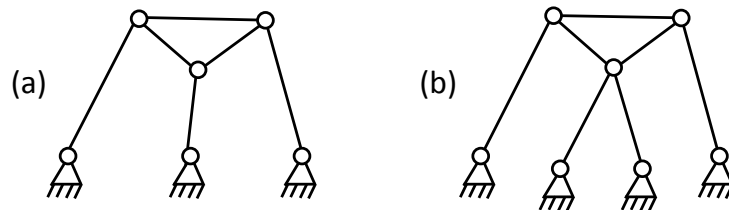


Figure 4.2: Classification of static trusses: (a) a statically determinate truss, and (b) a statically indeterminate truss.

There are two kinds of exceptions to this rule. The first kind is topological. For example, consider the structure in Figure 4.3. The number of bars is exactly twice the number of internal joints, yet bars 1-3 form a four-bar mechanism. The reason for this behavior is that this structure is built from two sub-structures: one is over-constrained (bars 4-8) while the other is under-constrained (bars 1-3). Together, the number of bars is equal to a well-constrained structure but it is not well-constrained.

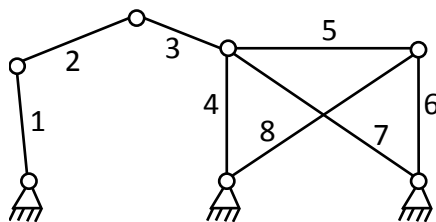


Figure 4.3: An example of a topological exception. The truss has $2j$ bars, yet it moves.

The second kind of exception, which is relevant to our work, is a geometrical exception. For example, consider the structure in Figure 4.4. The topology of this structure is the same as in Figure 4.2a. The geometrical characteristics of the structure are that bars 1, 4 and 6 are parallel and have the same length. Although the structure should be static according to the above rule, these characteristics make it a

mechanism. Actually, the structure is in a singular configuration (as explained in section 3.2). The singularity issue will be further discussed in the following sections.

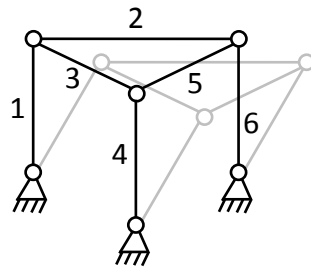


Figure 4.4: An example of a geometrical exception. Topologically, the structure is a statically determinate truss, yet it is mobile.

4.2 Assur trusses

The concept of the *Assur truss* was developed by Professor Leonid Assur at the Saint-Petersburg Polytechnic Institute. When first published in 1914, Assur's concepts did not receive much attention [18]. But in 1930 I.I. Artobolevskii, a leading member of the Russian academy of sciences, adopted Assur's approach and employed it in his widely used book [19]. From that time on Assur trusses were widely employed in Russia and other eastern European countries.

Assur trusses are a sub-group of statically determinate trusses and are defined as follows:

Let G be a statically determinate truss. G is an Assur truss IFF there is no sub-truss G' that is a statically determinate truss.

Figure 4.5a shows an example of an Assur truss. It does not contain any statically determinate sub-truss. This structure is called a *triad*. On the contrary, the truss in Figure 4.5b, although it is a statically determinate truss, is not an Assur truss since bars 1+5 form a statically determinate truss called a *dyad*.

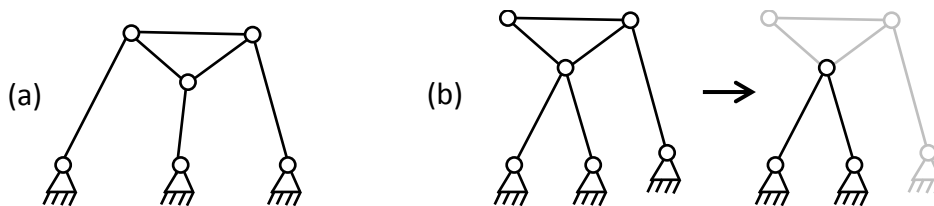


Figure 4.5: (a) An example of an Assur truss called a triad, and (b) a determinate truss with a sub-group which is a statically determinate truss (therefore it is not an Assur truss).

Every determinate truss which is not an Assur truss can be decomposed into Assur trusses [20]. For example, the determinate truss shown in the above figure can be decomposed into three dyads (which are Assur trusses) as shown in Figure 4.6.

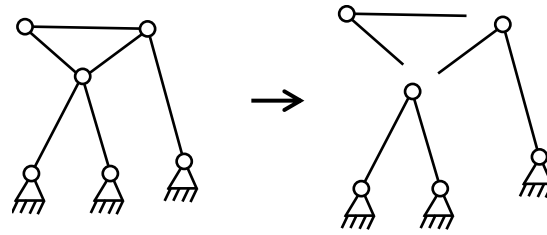


Figure 4.6: An example of the decomposition of a determinate truss into Assur trusses.

4.3 Assur tensegrity structures

One important property of Assur trusses [20], which is relevant to our work is given below:

For every Assur truss, there exists a configuration such that the truss has:

1. *A single self-stress, which is non-zero on all elements; and*
2. *A unique (up to scalar) first-order motion, which is non-zero on all inner joints.*

This special configuration is the singular configuration.

For the 2D triad shown Figure 4.5, the singular configuration is obtained when the continuations of the three ground legs intersect at a single point.⁵ Figure 4.7 shows a triad in a singular configuration. The intersection point O is also the momentary rotation center. Therefore the direction of the infinitesimal motion of each joint is perpendicular to the line connecting it to the intersection point O as shown in Figure 4.7a.

An Assur truss in a singular configuration can bear self-stress forces, as shown in Figure 4.7b. Thus, it can turn into a tensegrity structure: elements under tension can be replaced with cables, while elements under compression can be replaced with struts, as shown in Figure 4.7c. This sub-group of tensegrity structures is called *Assur tensegrity structures*. The same principles are true for three dimensional structures.

⁵ The structure in Figure 4.4 is in a singular configuration since its three legs intersect at infinity. Although singularity usually leads to infinitesimal motion, in this special case the motion is finite since the legs stay parallel during motion and singularity remains.

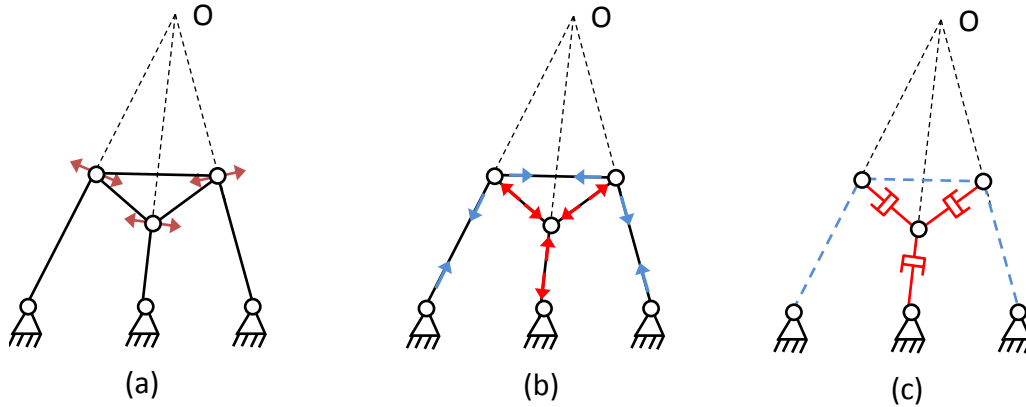


Figure 4.7: The singular configuration of a triad is characterized by the intersection of the continuations of the three ground legs: (a) the direction of the infinitesimal motion of the joints, (b) the self-stress forces, and (c) the Assur tensegrity structure.

Note that non-Assur determinate trusses can have configurations that fulfill one of the demands described in the above definition, but not both. Figure 4.8 shows two examples of non-Assur trusses in special configurations. The truss in Figure 4.8a is assembled from a triad in a singular configuration and a dyad on top of it. In this case all joints have infinitesimal motion, but the dyad on top is not self-stressed. The truss in Figure 4.8b, assembled from two dyads, has a self-stress in all of its elements, but only one joint is mobile.

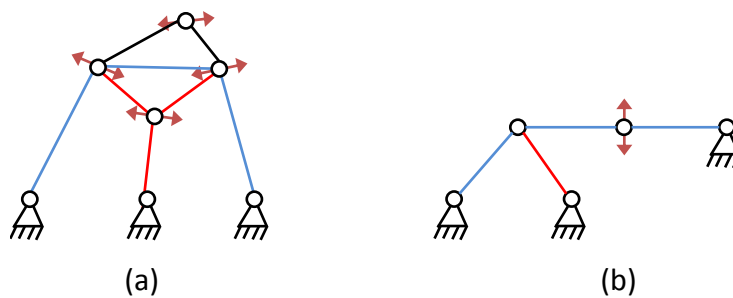


Figure 4.8: Special configurations of non-Assur determinate trusses: (a) a truss which has motion in all inner joints but doesn't have a self-stress in all elements, and (b) a truss which has a self-stress in all elements but doesn't have motion in all inner joints.

4.4 Shape change of Assur tensegrity structures

The significance of the property described above is that, in an Assur tensegrity device, if one member is stressed then *all* of the members are stressed and the device is rigid. In other words, to determine that an Assur truss is in a singular configuration, it is

sufficient to demonstrate that only one member is stressed. Shai [21] proved the following theorem:

Let T be an Assur truss in a generic position. For every ground element B_i there exists a length L_i' such that Assur Truss T' , generated by replacing element B_i with an element B_i' having length L_i' , is in a singular configuration.

According to this theorem, it is possible to make any Assur truss configuration into a singular one simply by changing the length of any one of its ground elements. Figure 4.9 demonstrates this theorem. Another conclusion is that when an Assur truss is in a singular configuration, the length of one element is determined by the length of all other elements.

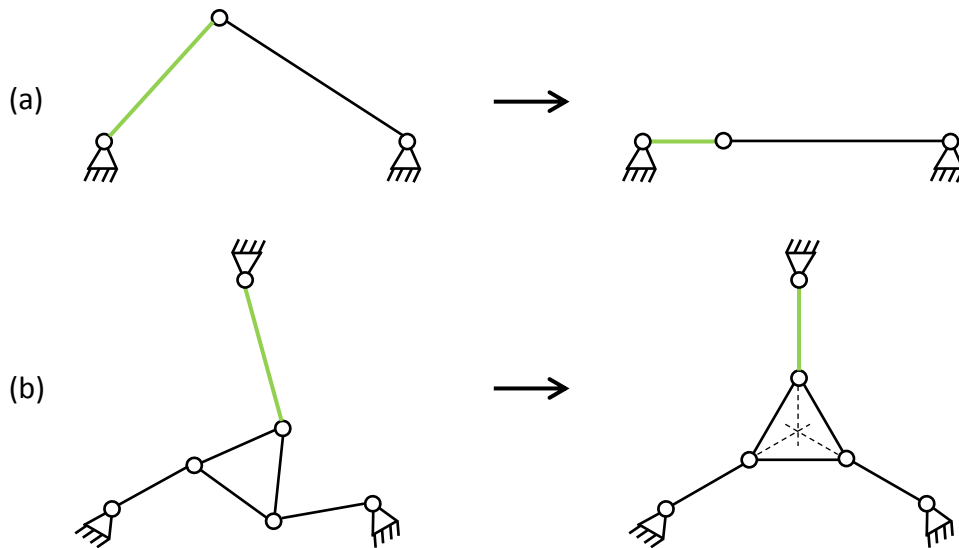


Figure 4.9: Singular configuration results from the change in length of only one ground element (colored in green): (a) in a dyad, and (b) in a triad.

Based on the above background, Bronfeld [22] developed the following shape change algorithm of an Assur tensegrity structure:

1. Choose one ground element to be the *force-controlled* element. All other elements are *position-controlled* elements.
2. Select the desired force in the force-controlled element. The forces in all other members will be proportional to the force in the force-controlled member (since the device has a *single* self-stress in all of its members).

3. Select a target shape for the device and calculate the target lengths of all position-controlled elements (the force-controlled length is dependent in their lengths).
4. Generate a trajectory for each position-controlled element according to their initial and final lengths (and according to the allowable speed and acceleration).
5. Activate the device controllers in the following manner:
 - The controller of the force-controlled member causes it to maintain the desired force, thus assuring the device's stiffness.
 - The controllers of the position-controlled members cause member lengths to follow their defined trajectories, thus changing the device's shape into the desired one.

The advantage of this algorithm over most others (two of them were described in section 3.6) is that it requires very little computation time. Only one singular configuration needs to be found (the target configuration), while other algorithms require that many singular configurations be found, changing progressively from the starting configuration to the target configuration. Also, the trajectory of each position-controlled element is independent of the rest of the elements, as opposed to the common approach that requires coordinated control of all actuators.

To test the algorithm, Bronfeld built a three dimensional triad robot, as shown in Figure 4.10. The robot has 6 controlled elements: 3 cables and 3 pistons. One cable was chosen as the force-controlled element while all other 5 are position-controlled. The experimental robot has confirmed the simplicity and robustness of the algorithm.

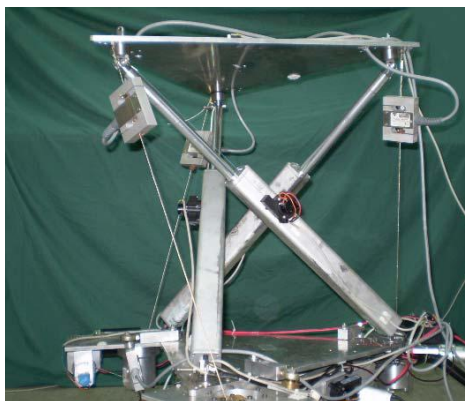


Figure 4.10: The experimental robot built for testing Bronfeld's shape change algorithm.

5 Model basics

This chapter starts with a description of the model segment and the construction of the complete mechanical model. It then analyzes the stability of several segment configurations. Conceptually, the stability analysis should precede model description, since the model employs the results of this analysis; nevertheless, for the sake of readability, the stability analysis will follow the model description.

Finally, it introduces two more important issues regarding the model segment: shape change and softness.

5.1 The mechanical model

5.1.1 The model segment

In our model, each segment of the biological caterpillar is represented by a planar tensegrity triad.

Compared to the standard tensegrity triad, the model triad has a few modifications that were made to simplify the model and to enable direct connection between segments: the model triad is rotated 90°; the top triangle is replaced with an un-actuated rigid bar and the ground supports are replaced by another bar (Figure 5.1). Note that the model triad is no longer a truss, but rather a structure.

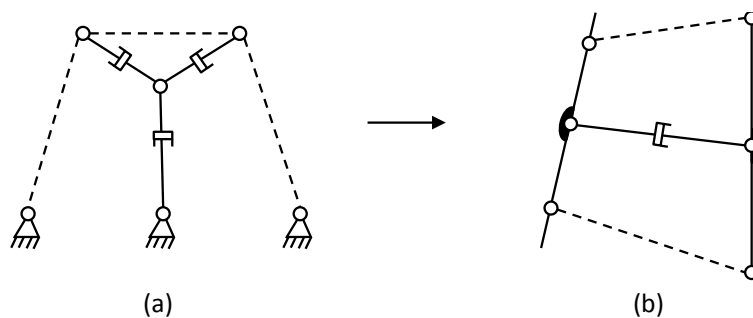


Figure 5.1: The standard triad in (a) as compared to the model triad in (b).

The three elements between the two bars of the model triad have controllable length and are referred to as the *actuated elements* (two cables and a strut).

Note that throughout the thesis the triad is sometimes illustrated as two vertical bars connected by two cables and a strut (as in the model) and sometimes as a horizontal

top bar connected by cables and a strut to three ground supports (resembling the standard triad). Either way there are always three actuated elements.

5.1.2 Legs

In contrast to other soft-bodied animals (worms for example), caterpillars interact with the environment via discrete contacts – their legs (prolegs in the abdomen and true legs in the thorax). Legs afford elevation, which avoids the necessity of dragging the body elements across the ground (with its concomitant friction and wear) and provide excellent traction. There is no need for the body to be raised in order to disengage the ground – the legs only need to be lifted. As mentioned in section 2.2, caterpillar legs are used as anchors rather than levers. When a leg touches the ground it cannot be lifted until it is actively unhooked and retracted.

In our model, legs are connected to the bottom of each bar and are inspired by the characteristics of the biological caterpillar proleg. They can be lifted or lowered; they are used as supports and not as levers. In addition, they also have the ability to grip the ground.

In contrast to the biological caterpillar which has three segments without legs, all of the model segments have legs. The reason for this change is to ease the caterpillar control and to make the movement more robust (see also section 9.2).

5.1.3 The complete model

The caterpillar model consists of eight segments connected in succession. This number of segments – eight – was chosen according to the number of *Manduca Sexta* abdominal segments (since the three thoracic segments are not necessary for locomotion [2]). Also, simulations have shown that eight segments are sufficient to perform robust and efficient crawl. Figure 5.2a shows the model as it seen in the simulation.

The model represents well the biological caterpillar: The upper cable represents the ventral longitudinal muscle (VL1), the lower cable represents the dorsal longitudinal muscle (DL1) and the strut, which is always subjected to compression forces, represents the hydrostatic skeleton. The vertical bars represent the antecostae (Figure 5.2b and Table 5.1).

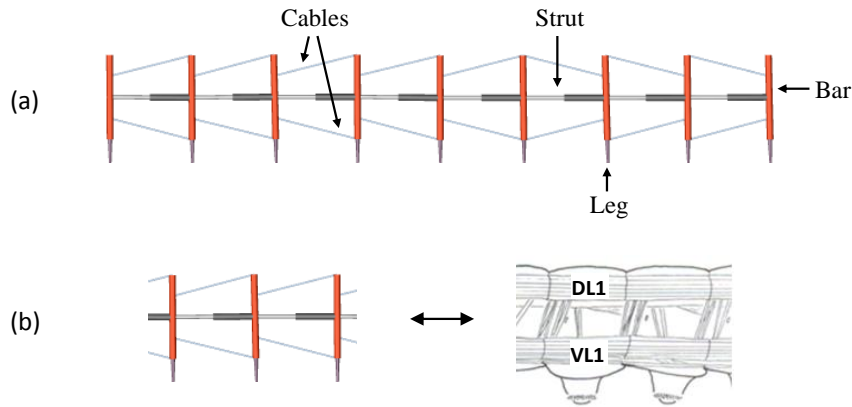


Figure 5.2: The caterpillar model: (a) The model is constructed of eight segments connected in succession, and (b) comparison between the model and the biological caterpillar.

Table 5.1: Comparison between a segment of the caterpillar model and that of the biological caterpillar.

Caterpillar Model	Biological caterpillar
Upper cable	VL1
Linear actuator	Hydrostatic skeleton
lower cable	DL1
Bars	antecostae

5.2 Stability

The following section describes a stability analysis of a triad.

5.2.1 The principle of potential energy

The stability of a tensegrity structure can be determined by applying the principle of potential energy, which states the following:

1. If a system is in equilibrium, the derivative of its potential energy must be zero. If the system has more than one degree of freedom, all the partial derivatives must be zero.
2. If the system is in stable equilibrium, the potential energy function is at its minimum point.

When an actuated element – cable or strut – changes its length, the change in potential energy of the system is as follows:⁶

$$\Delta U = - \int_{l_0}^{l_f} F(l) dl \quad (5.1)$$

where U is the potential energy, F is the internal force in the element and l is the length of the element. F is positive for compression forces and negative for tension forces.

We can illustrate this principle by considering a cable. When a cable is shortened, the tension force and the displacement have the same sign, and thus the potential energy of the system decreases. On the contrary, when the cable is lengthened, the force and the displacement have opposite signs and the potential energy of the system increases. A similar analysis for a compressed strut demonstrates that when it becomes shorter the potential energy decreases and vice versa.

Therefore, *to get a stable system, any shift from equilibrium must result in cable lengthening and/or strut shortening.*

5.2.2 Analyzing triad stability

A tensegrity triad is in equilibrium when the continuations of the three actuated elements intersect at a single point (See section 4.3). Two basic configurations that satisfy this condition are shown in Figure 5.3:

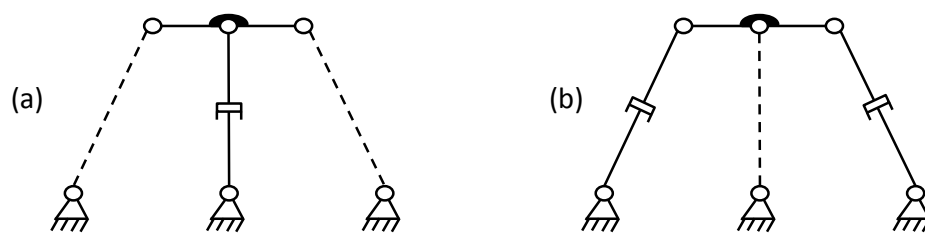


Figure 5.3: Two options for tensegrity triad configuration: (a) two cables and one strut, or (b) two struts and one cable.

This condition, however, does not guarantee equilibrium stability. To analyze the stability of a triad, the following method is suggested:

⁶ Note that there is no need to use the vector version of the formula since the force and the displacement are always on the same line.

At all times, two of the three actuated elements are assumed to be at constant length and therefore not influencing potential energy. The third element, referred to as the *tested element*, is allowed to change its length.

The two elements of constant length together with the top bar, form a 4-bar mechanism. Now, suppose that any shift of this 4-bar mechanism from equilibrium tends to lengthen the tested element. If this is the case, the tested element must be a cable if the system is to be stable. If, instead, the tested element tends to become shorter, the tested element must be a strut.

Case 1: The tested element is to the side (in this example, element O_3C). Consider that element O_2B has a rotational velocity ω as shown in Figure 5.4.⁷

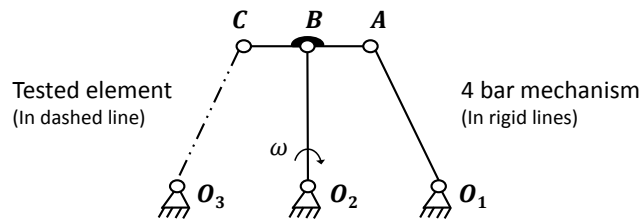


Figure 5.4: Stability analysis – case 1.

The velocity diagram of the triad is:

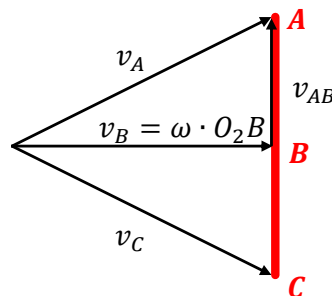


Figure 5.5: Velocity diagram of the triad.

The instantaneous velocity of point C is exactly perpendicular to the tested element (this can also be explained by the fact that the top bar's instantaneous center of rotation is placed on the continuation of all three elements). Thus, point C moves, instantaneously, in a circular motion around point O_3 , as shown in Figure 5.6.

⁷ In this example, the driving element O_2B has a velocity in the clockwise direction; the results are the same for counterclockwise velocity.

Therefore, velocity itself cannot tell us whether the element tends to become shorter or longer (because length is not changed in circular motion).

The next step is to check the acceleration of point C . In order to keep point C in pure circular motion around O_3 , the radial acceleration (the acceleration towards O_3 , as shown in Figure 5.6) must be equal to $\frac{v_c^2}{|O_3 C|}$. If acceleration is higher than this critical value, point C tends to become closer to point O_3 , and the tested element tends to become shorter. If acceleration is lower than this critical value, point C tends to become farther from point O_3 and the tested element tends to become longer.

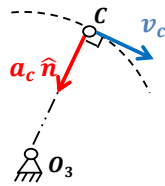


Figure 5.6: Velocity and radial acceleration of point C .

The acceleration diagram of the triad is:

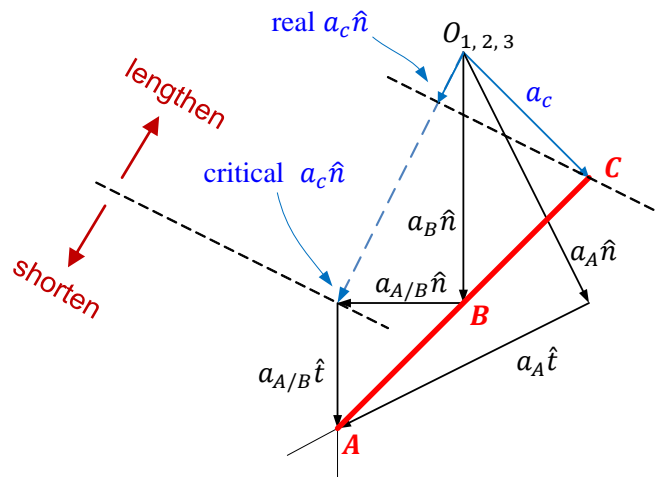


Figure 5.7: Acceleration diagram – case 1. The real radial acceleration of point C is lower than the critical radial acceleration.

The diagram shows that the real radial acceleration (real $a_c \hat{n}$) is lower than the critical radial acceleration. Thus, the tested element becomes longer when shifting from equilibrium. Therefore, for stable configuration, the tested element must be a cable.

Case 2: The tested element is in the middle (element O_2B) and element O_3C has a rotational velocity ω , as shown in Figure 5.8.

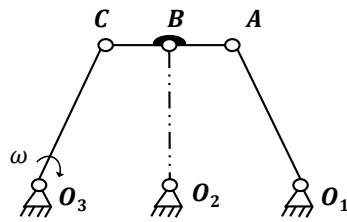


Figure 5.8: Stability analysis – case 2.

The velocity diagram is, again, insufficient to determine whether the tested element tends to become shorter or longer. The acceleration diagram for this case is shown in Figure 5.9:

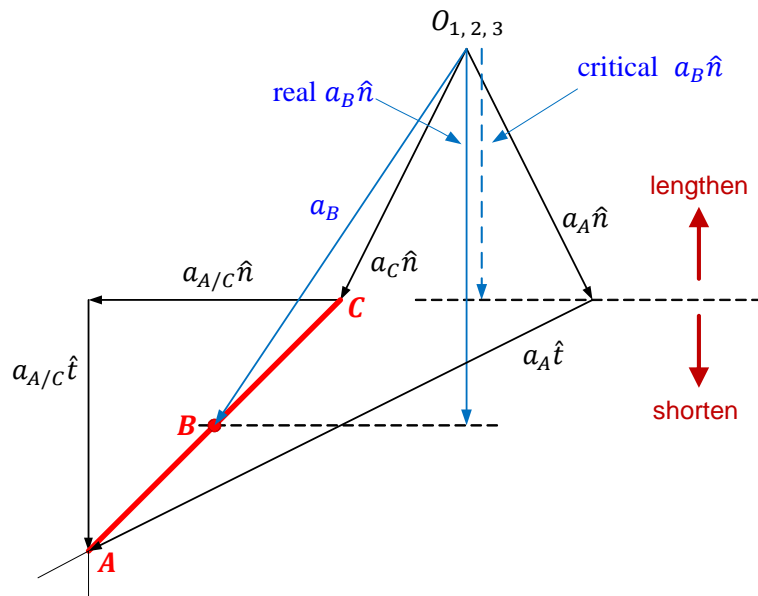


Figure 5.9: Acceleration diagram – case 2. The real radial acceleration of point B is lower than the critical radial acceleration.

The real radial acceleration (real $a_B \hat{n}$) is higher than the critical radial acceleration. Thus, the tested element becomes shorter when shifting from equilibrium. For stable configuration the tested element must be a strut.

Analysis of both cases demonstrates that the triad in Figure 5.3a is stable and that the one in Figure 5.3b is unstable.

5.2.3 Additional triad configurations

Two other options for a tensegrity triad are shown in Figure 5.10. In these configurations the elements are crossed and the intersection point is within the triad.

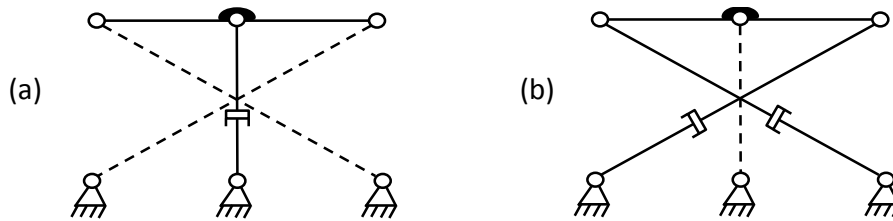


Figure 5.10: Two additional triad configurations.

Similar analysis for these configurations indicates that the triad in Figure 5.10b is the stable triad⁸ while the other is unstable.

The configuration we chose for our model is the one in Figure 5.3a since it is stable and resembles the caterpillar anatomy (as shown in Table 5.1).

5.3 Shape change

A method for determining the shape of the model triad is presented in this section. We will detail an algorithm which calculates the required element lengths for a desired triad shape - a process known as inverse kinematics.

The singularity of a triad is characterized by the intersection of the continuations of the cables and the strut at a single point. Note that this constraint reduces the degrees of freedom (DOFs) of the triad from three to two.

For calculation, one bar (called the base bar) is assumed to be fixed and the other bar (called the follower bar) is free to move. Nomenclature for the algorithm is shown in Figure 5.11.

⁸ A physical model of this configuration was built and tested in our lab.

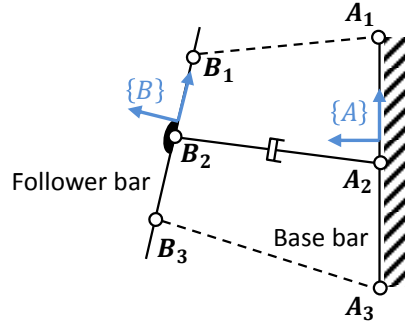


Figure 5.11: Nomenclature for the inverse kinematics calculation.

The details of the inverse kinematics algorithm are as follows:

1. Attach the base frame $\{A\}$ and target frame $\{B\}$ to the base and follower bars respectively.
2. Determine the desired position of the target frame relative to the base frame. Remember that the triad has only two DOFs, and therefore the angle of the target frame is dependent on its position.
3. The coordinates of the base connection points A_1, A_2, A_3 can be easily calculated since these points are rigidly connected to the base frame.
4. The coordinates of the follower connection points B_1, B_2, B_3 can be expressed by using the target frame position and the unknown target frame angle φ .
5. The line equation of an element i ($i = 1, 2, 3$) is:

$$(A_{iy} - B_{iy})y + (B_{ix} - A_{ix})x = A_{iy} \cdot B_{ix} - A_{ix} \cdot B_{iy} \quad (5.2)$$

6. The algebraic formulation of three lines that intersect at one point is represented by setting the determinant of their coefficients to zero:

$$\det \begin{pmatrix} A_{1y} - B_{1y} & B_{1x} - A_{1x} & A_{1y} \cdot B_{1x} - A_{1x} \cdot B_{1y} \\ A_{2y} - B_{2y} & B_{2x} - A_{2x} & A_{2y} \cdot B_{2x} - A_{2x} \cdot B_{2y} \\ A_{3y} - B_{3y} & B_{3x} - A_{3x} & A_{3y} \cdot B_{3x} - A_{3x} \cdot B_{3y} \end{pmatrix} = 0 \quad (5.3)$$

7. The above equation is a quartic equation with one unknown – φ . Solving this equation gives the angle φ .
8. Now having φ , the coordinates of the follower connection points B_1, B_2, B_3 can be precisely calculated.

9. The length of each element is:

$$l_i = |\mathbf{A}_i \mathbf{B}_i| = \sqrt{(B_{iy} - A_{iy})^2 + (B_{ix} - A_{ix})^2}, i = 1, 2, 3 \quad (5.4)$$

5.4 Softness

As mentioned in section 3.4, tensegrity structures have infinitesimal mechanism, and therefore exhibit infinitesimal deformation when subjected to external forces (regardless of the elastic deformation of each individual element). The control algorithm described in section 4.4 (in brief, one element is force-controlled while all others are position-controlled) increases this deformability – *it turns the infinitesimal mechanism into a finite mechanism*. Thus the mechanism demonstrates “softness” in that it deforms by external forces. This happens because the force-controlled element can change its length in response to external forces. This behavior is referred to as *structural softness* (as opposed to “regular” softness achieved by soft materials). This control algorithm will be referred to as the *basic control algorithm* from now on.

For example, suppose the force-controlled element is a cable and its tension is set to 1 Newton. If an external force causes the tension in the cable to increase, the cable will lengthen until tension is returned to 1N. When the external force disappears, the tension will be decreased, and the cable will shorten until it returns to its original length; the triad will return to its singular configuration.

Another important characteristic is that the degree of softness (meaning the degree of deformation) is proportional to the internal force in the force-controlled element. Therefore, a higher force in the force-controlled element decreases softness, and, vice versa, a lower force increases softness.

Figure 5.12 shows several simulations that demonstrate this behavior. In these simulations, the right bar is fixed while the left bar is subjected to three different forces. The upper cable and the strut are subjected to position-control and their lengths are constant. The lower cable is the force-controlled element.

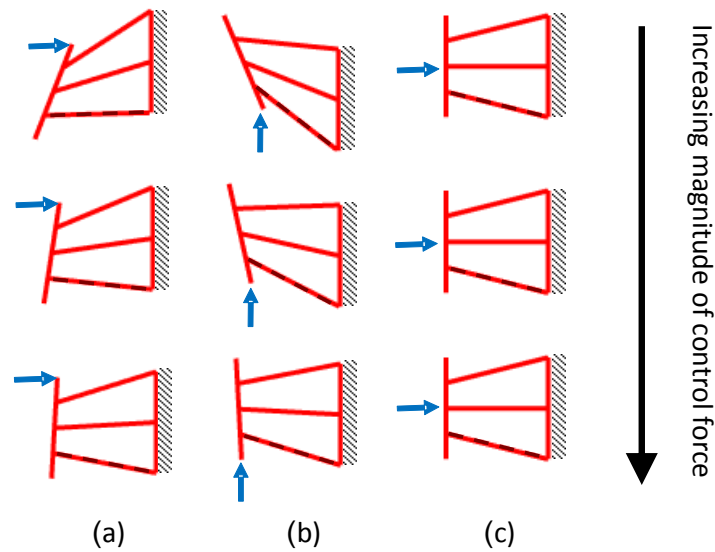


Figure 5.12: The effect of external forces on the triad shape. The force-controlled element is dashed. In (a) and (b) the effect of the external force decreases as the tension in the force-controlled cable increases. The force in (c) does not affect the triad since it does not apply any moment.

The forces in Figure 5.12a,b change the position of the bar. Nevertheless, as the tension in the force-controlled cable (the lower cable) increases, the effect of the external force decreases. The force in Figure 5.12c does not apply any moment to the instantaneous center of rotation of the bar (which is the intersection point of the three elements), and therefore does not affect the triad.

When an external force is acting on the triad, the inverse kinematics method described in section 5.3 is no longer valid. A geometric method was developed for characterizing the triad position when it is subjected to an external force acting on the center of mass of the bar (Figure 5.13):

1. Calculate the resultant force of the internal force of the force-controlled element and the external force ($F_{res} = F_{int} + F_{ext}$)
2. The action line of the resultant force passes through the intersection point of the action line of the two forces.
3. This action line and the continuations of the other two elements intersect at one point.

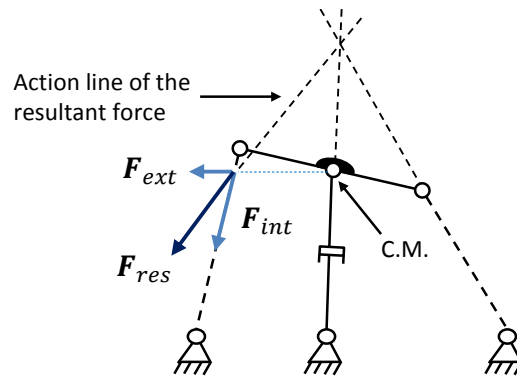


Figure 5.13: The change of the triad shape due to external force acting on the center of mass of the bar. The geometric characterization is that the continuations of the action line of the resultant force and the other two elements intersect at one point.

5.5 Chapter Summary

In this chapter we described the structure of the triad used to model a single segment of the caterpillar. The chapter also introduced the three main problems which are of concern in our mode: (1) stability, (2) shape change and (3) softness. The next chapter will introduce enhancements to the model triad and will further develop the three main issues listed above.

6 Model enhancements

This chapter introduces two improvements to the triad model: impedance control and area conservation. The motivation and the implementation of each of the two enhancements will be described. Also, their effect on the three problems of stability, shape change and softness, will be analyzed.

6.1 Impedance control

In general, robot degree of freedom (DOF) can be controlled by one of two control types: position control or force control (no mechanical system can determine both position and force). In position control, the control variables are kinematic: position, velocity and acceleration; in force control the control variable is the force which the robot exerts on the environment [23].

Motion control is useful for many industrial applications because of its high accuracy: each joint position is calculated and monitored at each point in time. Nevertheless, it is not well suited when the robot interacts with the surrounding environment, as do the segments of our model (with the ground and with the neighboring triads).

For example, consider the case of three triads (not necessarily tensegrity triads) between two walls, as shown in Figure 6.1. Any change in the length of any one element must be accurately coordinated with all other elements. (This is the case in Stulce's work mentioned in section 1.1). Uncoordinated movement can produce high forces with consequent damage to the robot. Therefore, the use of motion control in this case does not produce fault tolerance.

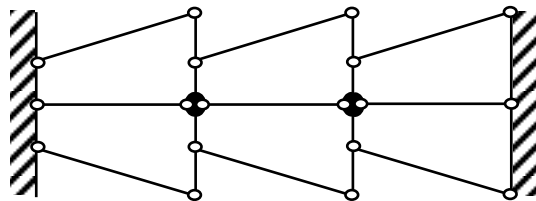


Figure 6.1: Triads between two walls.

Moreover, soft robots deform by external and internal forces, which makes it very difficult to coordinate their exact position. Our triad also demonstrates structural softness and possesses a similar problem.

In conclusion, pure motion control is not feasible for our model, and the suitable type of control for soft robots is force control.

6.1.1 Motivation for impedance control

Our basic control algorithm attempts to solve this problem by combining position control and force control – one element is force controlled while the two other elements are position controlled. As was demonstrated, this strategy enables deformation to external forces and therefore achieves some degree of fault tolerance.

But this “softness” is not sufficient. Consider the case that the two legs of the triad touch the ground (the connection of a leg to the ground is modeled by a revolute joint). In this case, the triad has zero DOFs even without the force-controlled element (Figure 6.2). Therefore, the force controlled element does not have any effect, and softness is lost.

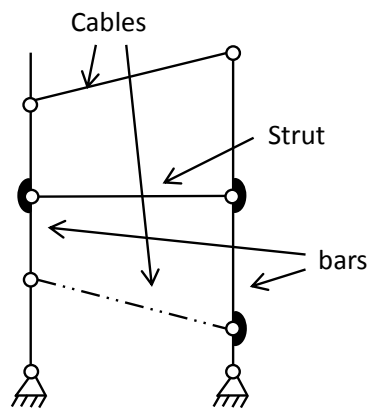


Figure 6.2: Illustration of the shortcoming of the basic control algorithm: The top cable and the strut are position controlled (represented as a rigid line) and the bottom cable is the force controlled element (represented as a dashed line). In that case when both legs touch the ground, the triad has zero DOFs and softness is lost.

One option is to add another force-controlled element: the two cables will be force controlled with a constant force on each cable. The strut will remain position controlled as shown in Figure 6.3.

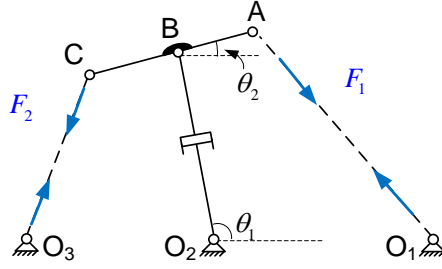


Figure 6.3: Two force-controlled elements.

Stability analysis for this control strategy was performed using the principle of potential energy (nomenclature is taken from Figure 6.3):

The strut is of constant length and does not affect the potential energy of the system. For simplicity, analysis was performed for the case that:

1. The cables are set to the same constant tension force $-F$, where F designates the absolute value of the force .
2. The geometric values are: $\mathbf{O}_1\mathbf{O}_2 = \mathbf{O}_2\mathbf{O}_3 = \mathbf{O}_2\mathbf{B} = a$, $\mathbf{AB} = \mathbf{BC} = a/2$

The potential energy of the system is given by:

$$U = \int_0^{l_1} F dl_1 + \int_0^{l_2} F dl_2 = F(l_1 + l_2) \quad (6.1)$$

Cable length can be described by:

$$\begin{aligned} l_1 &= a\sqrt{2.25 - 2 \cos \theta_1 - \cos \theta_2 + \cos(\theta_1 - \theta_2)} \\ l_2 &= a\sqrt{2.25 + 2 \cos \theta_1 - \cos \theta_2 - \cos(\theta_1 - \theta_2)} \end{aligned} \quad (6.2)$$

Now, Plotting $U(\theta_1, \theta_2)$ gives:

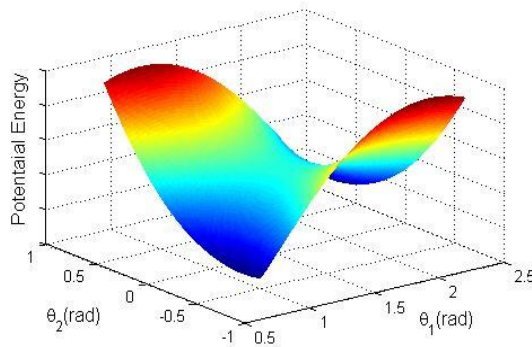


Figure 6.4: Potential energy graph of a triad with two cables under constant force control.

There is no minimum point on the graph. Therefore, the equilibrium point $[(\theta_1, \theta_2) = (\frac{\pi}{2}, 0)]$ is an unstable equilibrium point. The same result was also encountered in simulations of triads using other geometric and force conditions.

A new control strategy is needed and will be presented in the next section.

6.1.2 Introduction to impedance control

Physical systems can be divided into two types:

1. Impedances, which accept flow inputs (e.g., motion) and yield effort output (e.g., forces).
2. Admittances, which accept effort inputs and yield flow output.

The concepts of impedance and admittance are familiar to designers of electrical systems and are usually regarded as equivalent and interchangeable representations of the same system, which is true for all linear systems operating at finite frequencies. But manipulation is fundamentally a non-linear problem, and for non-linear systems this equivalence is not valid. For example, consider a manipulator that interacts with a constrained inertial object like a wall. The wall can be pushed but it can't be moved. Therefore, the manipulator can determine the output force but not the position. This and other examples show that *to ensure physical compatibility, the manipulator should assume the behavior of an impedance.*

The general strategy of impedance control is to control position (as in conventional robot control) and, in addition, to give “disturbance response” for deviations from that motion in the form of impedance. The standard impedance control law in industrial robots is:

$$\mathbf{F} = \mathbf{k}(\mathbf{x}_0 - \mathbf{x}) + \mathbf{b}(\mathbf{v}_0 - \mathbf{v}) \quad (6.3)$$

Where \mathbf{F} is the end point output force vector, \mathbf{x}_0 and \mathbf{v}_0 are the desired equilibrium end point position and velocity vectors in the absence of environmental forces (referred to as the *virtual position* and the *virtual velocity* respectively) and \mathbf{x} and \mathbf{v} are the real position and velocity vectors.

The lowest order term in any impedance is the static relationship between the output force and the input displacement, also known as stiffness, where \mathbf{k} is the stiffness matrix. This term causes a spring-like behavior. The degree of stiffness can be controlled by changing the stiffness matrix.

The second term is the relationship between force and velocity, where \mathbf{b} is the damping matrix. It functions as a damper to moderate the manipulator's reaction time and to avoid fluctuations.

In standard industrial robotics, the above equation needs to be transformed from end point coordinates to joint coordinates by using the Jacobian matrix. Also, the inertial, frictional, and gravitational dynamics of the manipulator are sometimes taken into consideration [24].

6.1.3 Implementation of impedance control

The impedance control law used to actuate cables and struts in our model is a modification of the standard equation:

$$F = F_0 + k(l_0 - l) - bv \quad (6.4)$$

Where:

F - Output force

F_0 - Initial force

k - Stiffness coefficient

l_0 - Virtual length

l - Real length

b - Damping coefficient

v - Real velocity

The differences between the standard impedance equation and the one implemented in our model are as follows:

1. The main difference is the addition of initial force (F_0), which does not exist in the standard equation. This term is responsible for keeping the triad in self-stress. Of course, F_0 must be negative for cables (tension force) and positive for struts (compression force).
2. In the tensegrity triad each actuated element is controlled separately and independently. Therefore all variables in the equation are scalars rather than vectors or matrices.
3. There is no need to transform the equation from end point coordinates to actuator coordinates, and there is no need to consider robot dynamics. The equation above is sufficient as is.

4. Virtual velocity is omitted. This is warranted because caterpillar movement is relatively slow and virtual velocity can be considered as nonexistent; the final term is functioning as pure damping.
5. Finally, there is a nomenclature change: l is used instead of x .

6.1.4 Stability

As demonstrated in section 6.1.1, controlling both cables of the triad with constant force results in an unstable system. Repeating the analysis, this time with both cables under impedance control, gives a potential energy function of:

$$U = \int_0^{l_1} (F_0 + k(l_0 - l_1)) dl_1 + \int_0^{l_2} (F_0 + k(l_0 - l_1)) dl_2 = \quad (6.5)$$

$$(F_0 + kl_0) \cdot (l_1 + l_2) - \frac{1}{2}k \cdot (l_1^2 + l_2^2)$$

Plotting the graph yields:

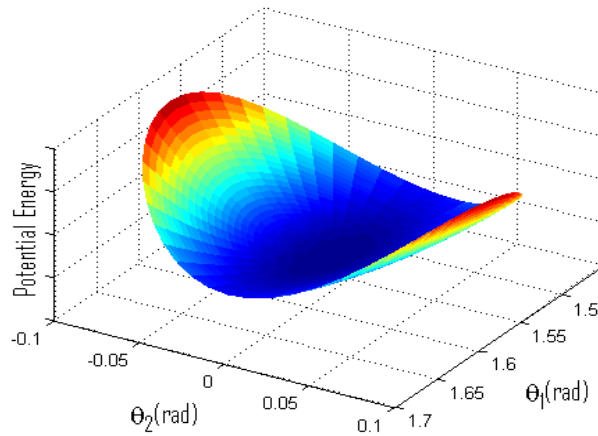


Figure 6.5: Potential energy graph of a triad with two cables under impedance control.

This time the graph has a minimum point and, therefore, the system is stable. Note that the stability is a function of k . Simulations indicate that there is a critical value of k below which the system is still unstable. This is because the output force gets closer to the situation of constant force as k becomes lower ($k = 0$ means constant output force if the transient damping is neglected).

Also, simulation shows that stability remains when all three elements – the cables and the strut – are under impedance control (no graph is shown due to the difficulty of visualizing a function with three variables).

6.1.5 Shape change

The final shape of the triad is achieved when it reaches its equilibrium point. Changing the impedance control parameters F_0 , k and l_0 changes the equilibrium point and therefore causes the triad to change its shape. (The parameter b doesn't influence the final equilibrium; it only influences the transition between two shapes.) Remember that each actuated element is controlled separately, and different elements can have different parameter values.

Note that although the impedance equation is controlled by four parameters, two parameters – F_0 and l_0 – are redundant and three parameters are sufficient to explicitly determine element behavior. For example, the following two impedance equations are identical:

1. $F_0 = 1, l_0 = 3, k = 2, b = 1 \rightarrow F = 1 + 2(3 - l) - v = 7 - 2l - v$ (6.6)
2. $F_0 = 3, l_0 = 2, k = 2, b = 1 \rightarrow F = 3 + 2(2 - l) - v = 7 - 2l - v$

Nevertheless, it is very convenient to use the impedance equation as it appears in equation (6.4) for the following reasons:

1. The impedance equation emphasizes the self-stress forces. When the actuated element is at its virtual position, the output self-stress force is F_0 .
2. More importantly, the impedance equation enables more intuitive control of triad shape: F_0 is responsible for the base forces of the triad and l_0 is responsible for controlling the element length.

6.1.6 Softness

When all three actuated elements of the triad are under impedance control, the triad exhibits much higher deformability than it would using the basic control algorithm since each element can change its length when the triad is subjected to external forces. For example, look again at Figure 5.12c. The horizontal force in the middle of the bar had no effect on the triad shape when using the basic control algorithm. When using impedance control in all elements, this force causes the triad to shrink.

The stiffness (or softness) of the triad can be controlled by changing the stiffness coefficient. Increasing the stiffness coefficient (k) in all elements increases the overall

stiffness of the triad. Decreasing k will result in a loose triad. Analytical analysis of triad shape change and softness will be discussed in section 6.3.

6.2 Area conservation

6.2.1 Nomenclature

The common way to specify a rigid body position in a plane is by its two Cartesian values (x,y) plus a rotation angle. This section presents a different and bijective way of doing so, which will be used later in this chapter.

Look at the two frames shown in Figure 6.6 . l is the distance between the two frame origins, ϕ_1 is the angle from the positive x -axis of frame $\{A\}$ in a CCW manner to the positive direction of the connection line, as shown in the figure. ϕ_2 is similarly defined.

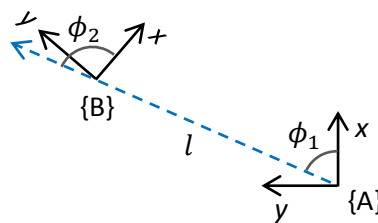


Figure 6.6: Describing a frame in plane.

Now, the position of frame $\{B\}$ relative to frame $\{A\}$ can be explicitly described by the following three parameters:

l – The distance between the frame origins

φ_B – Bending angle, defined as $\frac{\phi_2 - \phi_1}{2}$

φ_S – Shear angle, defined as $\frac{\phi_2 + \phi_1}{2} - 90^\circ$

To understand the meaning of the angles, consider the segments described in Figure 6.7. The frames are attached to the bars such that their x -axis is placed along the bar. For clarity, only bars and struts are illustrated.

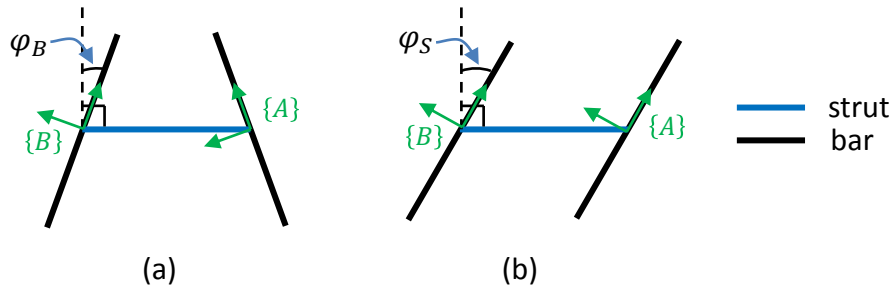


Figure 6.7: Segments subjected to pure bending (a) and pure shear (b).

The segment in Figure 6.7a is subjected to pure bending (shear angle is 0°). A segment under pure bending forms an isosceles trapezoid. On the contrary, the segment in Figure 6.7b is subjected to pure shear (bending angle is 0°). A segment under pure shear forms a parallelogram.

6.2.2 Motivation for area conservation

Figure 6.8 shows two examples of a caterpillar simulation. The actuated elements are all impedance controlled. The model in Figure 6.8a is subjected to a gravitational force horizontal to the caterpillar (e.g., when climbing up a wall), which makes the caterpillar lean. Two consecutive legs are lifted in Figure 6.8b, and their segments fall to the ground. In both examples simulations show that *the model is sensitive to shear movement*, meaning that relatively small forces can result in large shear movements. Other examples can be found which demonstrate this problem.

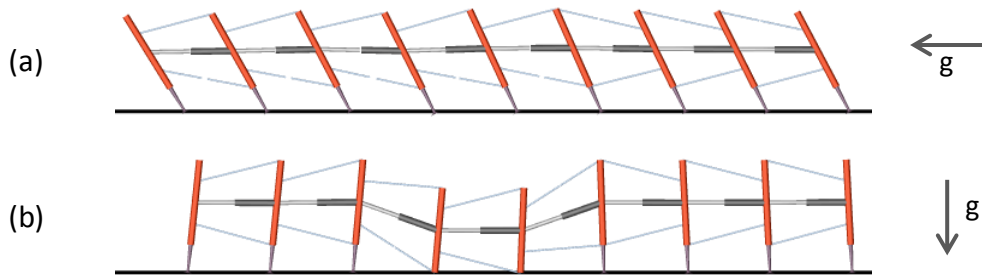


Figure 6.8: Two examples demonstrating that the model is too sensitive to shear movement.

One way to solve this problem is to increase the stiffness of the segments by increasing F_0 and k parameters. But doing so undermines the principal property of the model – its softness. The following section describes an alternative method.

6.2.3 Implementation of area conservation

One might ask why this phenomenon is not a problem for the biological caterpillar. The answer is that caterpillars have nearly constant volume (the internal air cavity that can be emptied constitutes 3-10% of body volume [25]), and this volume conservation in the real caterpillar does not allow shear deformation.

Because our caterpillar model is a two dimensional model, we employ area rather than volume conservation.

The shear angle φ_s has an impact on the caterpillar area. The area of a segment in pure shear is shown in Figure 6.9 and given by:

$$S = ab \cos \varphi_s \quad (6.7)$$

The change in area relative to the maximum area for a small shear angle is:

$$\Delta S = ab(1 - \cos \varphi_s) \approx \frac{1}{2}ab \cdot \varphi_s^2 \quad (6.8)$$

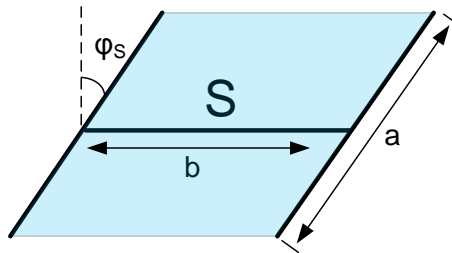


Figure 6.9 : Segment area in pure shear

To avoid this shear movement and its consequent area loss, *internal torque* is added to the joints connecting the strut and the bars as shown in Figure 6.10.

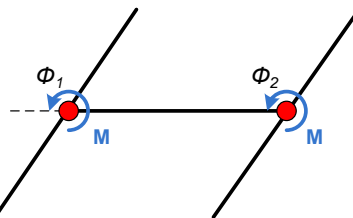


Figure 6.10: Internal torque is applied to the joints connecting the strut and the bars.

The internal torque resists the area loss ΔS and its value is proportional and opposite to the shear angle:

$$M_i = -c \cdot \phi_s \quad (6.9)$$

This internal torque is calculated and applied to each segment separately. Simulations under the same conditions as those in Figure 6.8 and with the additional internal torque are shown in Figure 6.11. It can be seen that the model is now more rigid.

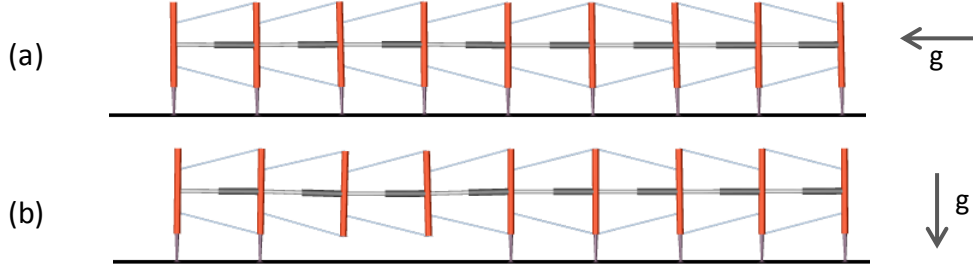


Figure 6.11: The effect of internal torque.

Note that although segment area is also determined by the bending angle (ϕ_B) and the strut length (l), their effect is minimal:

- During crawl most segments undergo little bending. Therefore, the bending angle ϕ_B has little effect on the total caterpillar area.
- Although l clearly affects segment area, when the entire model is considered, some segments are shrunken and some are stretched such that the overall length of the model is nearly constant. Therefore, l does not greatly affect caterpillar area (see section 8.5.1).

Also, observation of biological caterpillar movement shows that its segments do bend and shrink but do not cause significant shear deformation.

6.2.4 Stability

The potential energy of a tensegrity triad with two impedance-controlled cables is given in 6.1.4. The internal torque addition to this equation is:

$$\Delta U = - \int_0^{\phi_s} M_i d\phi_s = - \int_0^{\phi_s} -c\phi_s d\phi_s = \frac{1}{2}c\phi_s^2 \quad (6.10)$$

The total potential energy is given by:

$$U = (F_0 + kl_0) \cdot (l_1 + l_2) - \frac{1}{2}k \cdot (l_1^2 + l_2^2) + \frac{1}{2}c\phi_S^2 \quad (6.11)$$

Plotting this equation gives:

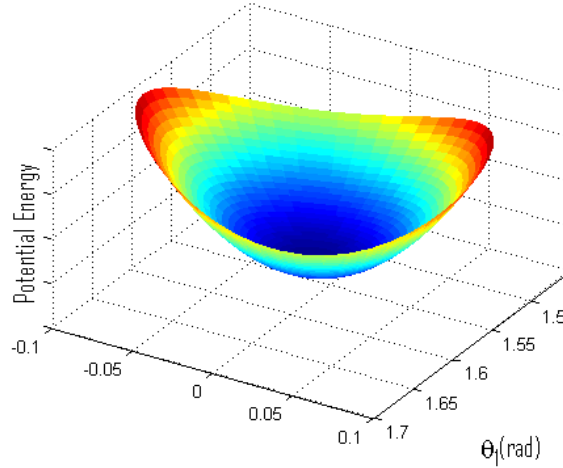


Figure 6.12: Potential energy graph of a triad with two cables under impedance control and internal torque.

If we compare this graph to that in Figure 6.5, we see that the minimum point remains and the graph becomes more convex. This means that the internal torque makes the stability more robust.

6.3 Final segment model

The final segment model has the following characteristics:

1. Cables are connected to the ends of the bars. This cable configuration resembles the configuration of the VL1 and DL1 muscles (see Figure 5.2b) and is much easier to analyze. This configuration is the one that will be used from now on. Note that this configuration is not possible without the internal torque because this would result in a finite mechanism (see Figure 4.4).
2. The internal torque coefficient c is high enough that the shear angle can be neglected. Therefore, the segment experiences pure bending, and assumes the shape of an isosceles trapezoid. Also, cables always stay parallel to the strut, as shown in Figure 6.13.

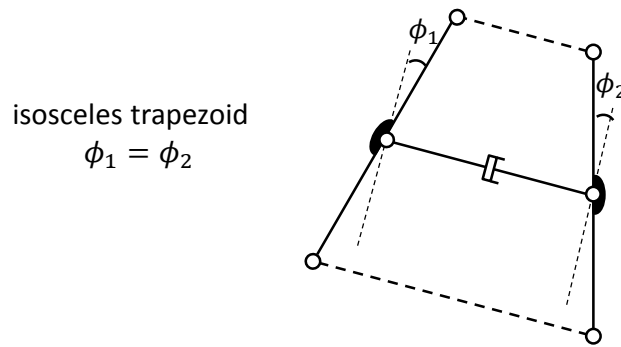


Figure 6.13: Final segment model: cables are connected to the ends of the bars, segment assumes the shape of an isosceles trapezoid and cables are always parallel to the strut.

3. The elements are under impedance control as follows (see also section 7.2):

- The strut control law:

$$P = F_0 - bv \text{ (the stiffness coefficient equals zero)}$$

- The cable control law:

$$T_1 = -\frac{F_0}{2} + k_1(l_1 - l_{0,1}) - bv \text{ and } T_2 = -\frac{F_0}{2} + k_2(l_2 - l_{0,2}) - bv$$

Note that F_0 and b are equal among all three elements, and the initial force of the cables is exactly half the magnitude of the initial force of the strut.

The internal torque changes the behavior of the triad, and the equilibrium conditions that was described in sections 5.3-5.4 are no longer valid. The following two sections present an analytical way to determine the shape of a triad with the impedance control and internal torque addition: section 6.3.1 analyzes shape change without external forces, and section 6.3.2 analyzes the effect of external forces (meaning softness). These sections show only the final results. The full development of the equations can be found in Appendix A. Figure 6.14 illustrates all the lengths, forces, torques and reactions that a segment possesses and which will be used in our analysis. For clarity, all elements are shown as rigid lines and joints are omitted.

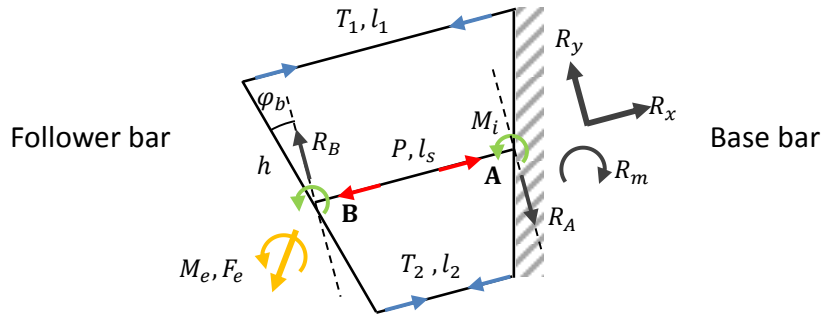


Figure 6.14: Segment lengths, forces, torques and reactions.

Where:

- h – Bars lengths
- l_1, l_2 – Cables lengths
- l_s – Strut length
- M_e, F_e – External torque and force acting on the center of mass of the follower bar
- M_i – Internal torque (torque is the same at both points)
- P – Strut force
- R_x, R_y, R_m – Reactions between the base bar and the wall
- R_A, R_B – Reactions between the strut and the bars (perpendicular to the strut)⁹
- T_1, T_2 – Cables tension
- φ_b – Bending angle

6.3.1 Shape change

Without external forces, the cables assume exactly the virtual lengths:

$$l_1 = l_{0,1} \quad , \quad l_2 = l_{0,2} \quad (6.12)$$

It is convenient to describe the shape of the triad by the two parameters - φ_b and l_s - which equal:

$$\varphi_b = \sin^{-1} \left(\frac{l_{0,1} - l_{0,2}}{2h} \right) \quad , \quad l_s = \frac{l_{0,1} + l_{0,2}}{2} \quad (6.13)$$

Note that the shape of the triad is determined only by the two virtual lengths of the cables ($l_{0,1}$ and $l_{0,2}$); the stiffness coefficients of the cables (k_1 and k_2) do not have any effect.

⁹ Normally, elements that are connected only at their ends do not exert perpendicular reactions. These reactions exist because of the internal torque.

The internal forces of the triad are as follows:

$$\begin{aligned} T_1 = T_2 = \frac{F_0}{2}, \quad P = F_0 \\ M_i = 0 \end{aligned} \quad (6.14)$$

Equilibrium is established when cable lengths are equal to virtual length and have the same tension (which is exactly half the strut force). Also, the internal torque has no effect and equals zero.

6.3.2 Softness

This section analyzes the effect of external forces on the triad shape.

In the general case an arbitrary force and torque are applied to the center of mass of the follower bar, and cables can have different virtual length and stiffness coefficients.

The analysis is performed only for the case that both cables have the same virtual length ($l_{0,1} = l_{0,2}$) and the same stiffness coefficient ($k_1 = k_2$), which will be denoted as l_o and k respectively. Also, analysis is performed for three distinct cases as shown in Figure 6.15.

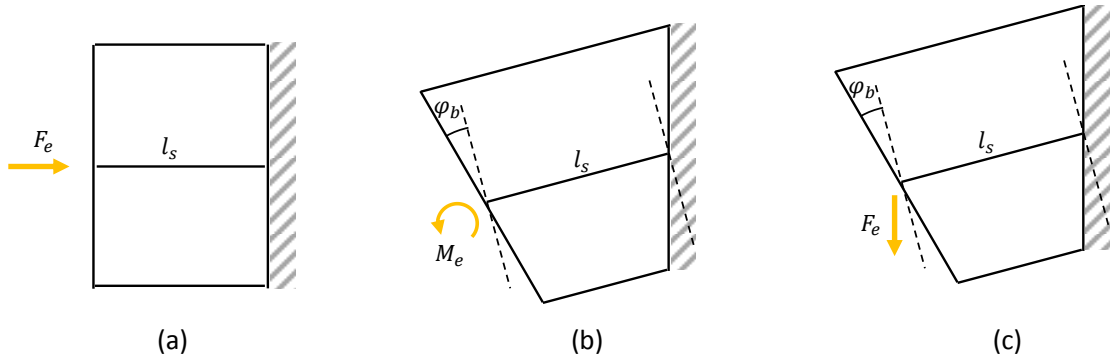


Figure 6.15: Three cases of external load: (a) axial force, (b) bending torque, and (c) bending force.

As mentioned, it is convenient to describe the shape of the segment by l_s and φ_b . Equations (6.15)-(6.16) give these two parameters for each of the three cases. Also, the maximum external load that can be applied is given. Beyond that maximum, at least one cable becomes loose, and the segment loses its stability.

(a) Axial force:

$$\begin{aligned} l_s &= l_0 - \frac{F_e}{2k} \\ \varphi_b &= 0 \\ F_e &< F_0 \end{aligned} \quad (6.15)$$

(b) Bending torque:

$$\begin{aligned} l_s &= l_0 \\ \varphi_b &\approx \frac{M_e}{kh^2} \\ M_e &< \frac{F_0 h}{2} \end{aligned} \quad (6.16)$$

(c) Bending force:

$$\begin{aligned} l_s &\approx l_0 \\ \varphi_b &\approx \frac{l_0 F_e}{2kh^2} \\ F_e &< \frac{F_0 h}{l_0} \end{aligned} \quad (6.17)$$

In all cases, cables length can be calculated as follows:

$$\begin{aligned} l_1 &= l_s + h \sin \varphi_b \\ l_2 &= l_s - h \sin \varphi_b \end{aligned} \quad (6.18)$$

Looking at the above equations, it can be seen that segment stiffness is determined (in part) by the stiffness coefficient k , not by the initial force F_0 . In contrast, the external load limit is dependent on the initial force but not on the stiffness coefficient. In other words, as long as the external load is within its limits, the initial force within the segment doesn't influence segment stiffness.

Interestingly, Lin, et al. [26] found that during caterpillar growth, in which caterpillars increase their body mass 10,000 fold, body pressure stays almost constant. Body pressure does not have a significant impact on caterpillar stiffness.

Moreover, they found that, as expected, muscle activation has a major effect on caterpillar stiffness. In our model, muscle activation is simulated, in part, by changing the stiffness coefficient (k) of the cables (described in detail in section 7.2.2). The equations above indicate that k has a major effect on segment stiffness.

¹⁰ This external force limit is relevant only for compression forces.

6.3.3 Determining the magnitude of the internal torque coefficient

In the previous section it was assumed that the internal torque coefficient c was sufficiently high that the shear angle could be neglected and the segments would assume the shape of an isosceles trapezoid. This assumption simplified the analytical considerations above.

Unfortunately, this also results in unwanted behavior.

To understand the problem, consider the case where a segment is connected to the ground. In this case, the isosceles trapezoid shape constraint leaves the segment with only one DOF – the bending angle – as shown in Figure 6.16.

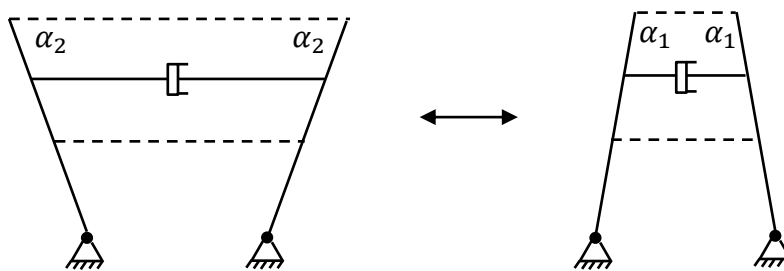


Figure 6.16: A grounded segment has only one DOF.

Now, several connected segments still have only one DOF. Changing an angle of one segment necessarily changes the angle of all other segments. For example, in Figure 6.17 the caterpillar stands on flat terrain with its right leg lifted (for clarity, the struts and bottom cables are not drawn). In Figure 6.17a the shapes of the caterpillar segments fit the terrain. But changing the angle of the right segment changes the shape of all other segments, shrinking and expanding them alternately, as shown in Figure 6.17b. Clearly, this shape is unwanted.

Note that this explanation is purely kinematic. Dynamically, trying to change the shape of the caterpillar model by controlling the right segment alone will simply not work: the rest of the segments will resist the change.

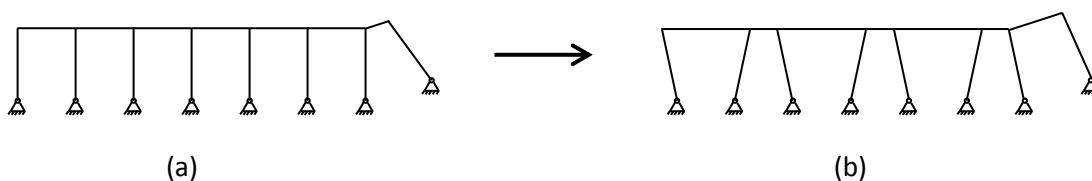


Figure 6.17: The problem of high c when several segments are grounded.

This can be resolved by lowering the internal torque coefficient (c) in a way that will enable a small (but not negligible) shear angle. In this way the effect of changing the angle of one segment will be damped in neighboring segments, as shown in Figure 6.18. The exact magnitude of c in our model was determined empirically.

Note that, when decreasing c , we can no longer assume isosceles trapezoid shape and the equations of the previous section are no longer valid. Nevertheless, simulations demonstrate that these equations still give good results.

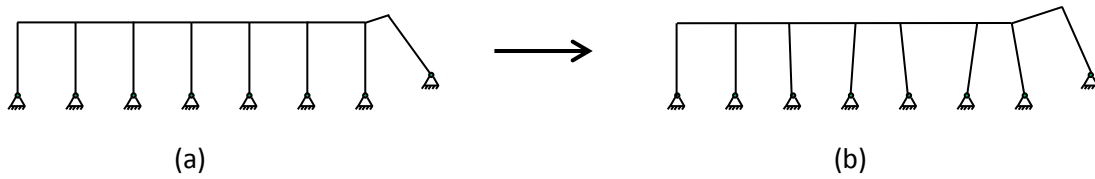


Figure 6.18: Using a c that enables a small shear angle solves the problem.

7 Caterpillar Control

As mentioned in section 2.1, caterpillars have a relatively simple nervous system; yet, they are able to execute complex maneuvers. Our control algorithm attempts to approximate caterpillar physiology and takes inspiration from its general structural concept.

The internal sensors the model uses are force and position sensors for each controlled element. Also, angle sensors for the determining the angles between each bar and its adjacent struts are used. The model does not employ vision techniques; the only external sensors used are ground contact sensors.

7.1 Control Scheme

Caterpillar control is divided into two major units:

1. High-level control delivers commands to the low-level controllers in order to effect coordinated motion. In this way, the high-level unit simulates the function of the nervous system.
2. Low-level control is composed of localized controllers for each of the cables, struts and legs, simulating the mechanical properties of the caterpillar. Each low-level controller is independent of all other low-level controllers: the controller output of an element – cable, strut or leg – is calculated using only the inputs of that specific element and, if needed, input from the high-level control unit.

The role of each type of the low-level controller is as follows:

- Cable controllers: Cables are analogous to muscles. The cable controllers mimic the mechanical behavior of the muscles. These controllers are directly controlled by the high-level control unit just as muscle activity is controlled by the nervous system.
- Strut controllers: Struts are analogous to the hydrostatic skeleton, and the strut controllers mimic hydrostatic pressure. These controllers are completely independent and are not controlled by the high-level control unit.

- Leg controllers: Leg controllers take on three roles: 1. to lift and lower the leg, 2. to control grip, and 3. to notify the high-level control unit that a leg is touching the ground. Leg controllers are controlled by the high-level control unit.

From the above, the high-level control unit controls the cables and legs but not the struts. High-level control is divided into two levels:

- Level 1 control: This is the central control unit and is inspired by the caterpillar's central pattern generator (CPG). Its role is to control movement timing and to activate the relevant cables and legs.
- Level 2 control: This mediates between level 1 control and the cable controllers of each segment, adjusting level 1 control for each segment according to terrain. Segment control is thus local, as inspired by caterpillar segmental ganglia.

Note that legs are directly controlled by the CPG and do not need this mediation since they have only two states.

An essential property of high-level control is that the coordination of locomotion is triggered by the contact of the legs with the ground. Figure 7.1 illustrates the hierarchy of the control scheme.

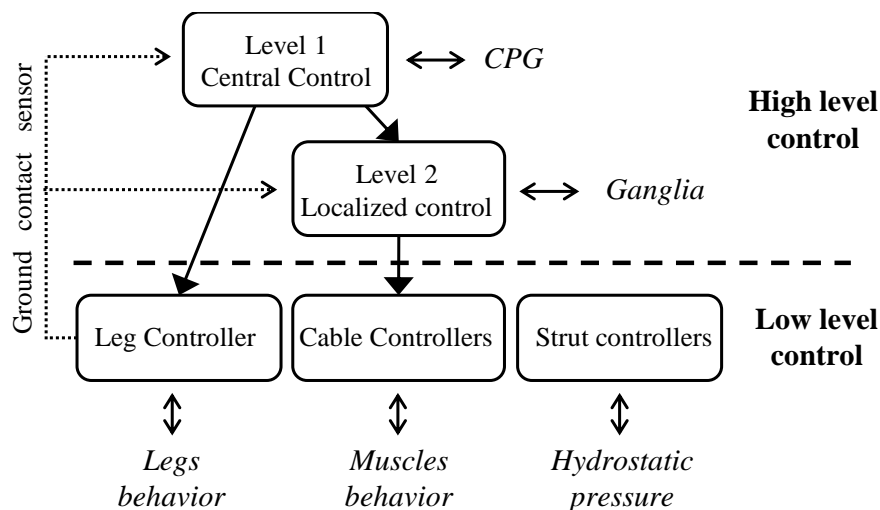


Figure 7.1: Hierarchy of the control scheme

7.2 Low-level control

Cables and struts are controlled by impedance, but the implementation of impedance control is different for each element.

7.2.1 Struts

Struts simulate the internal pressure of the caterpillar's hydrostatic skeleton. In the biological caterpillar the internal pressure is not constant, and the changes in pressure cannot be correlated with movement [25]. For simplicity, our model assumes constant pressure. Therefore, the stiffness coefficient k is set to zero and the control law for struts is reduced to:

$$P = F_0 - bv \quad (7.1)$$

where P is the output strut force and F_0 has a positive value (compression force).¹¹ The parameters of the strut controllers (F_0 and b) are constant during all stages of simulation.

7.2.2 Cables

Cables simulate the function of caterpillar muscles. Caterpillar muscles have a large, nonlinear, deformation range and display viscoelastic behavior. Figure 7.2 illustrates muscle behavior in passive (also called *tonic*) state and fully stimulated (also called *tetanus*) state [27].

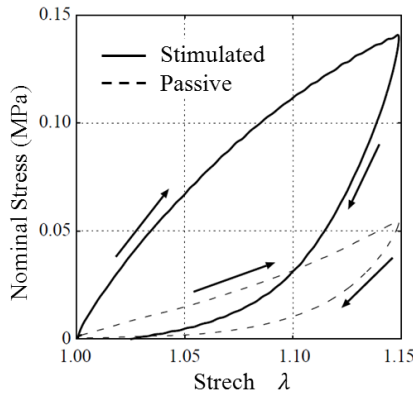


Figure 7.2: Experimental data for loading–unloading response of caterpillar muscle in passive and stimulated conditions.

The cable control law is:

¹¹ The output force is not truly constant because of the damping term. Nevertheless, it is nearly constant.

$$T = -\frac{F_0}{2} + k(l - l_0) - bv \quad (7.2)$$

Notice that the virtual force of a cable has a magnitude of exactly half the strut force and an opposite direction (tension force). The reason for this choice of the virtual force is that it enables a simple way to control segment shape: when there are no external forces, the cable lengths are exactly the virtual length (see section 6.3.1).

If all of the controller parameters (F_0 , k , l_0 and b) remain constant, the model will stay in a steady state and will not move. To control cable behavior, the cable controller receives an input signal from the high-level control (referred to as a *high-level command*). The ‘command’ input receives values between 0 and 1, which causes a change in the controller parameters and therefore changes cable behavior. In particular, the parameters that are changed due to the command input are k and l_0 , while F_0 and b are constant during all stages of simulation.

As high-level control simulates the nervous system and cables simulate the muscles, the high-level command simulates nerve stimulation. A command value of 0 indicates that the cable should be "relaxed," meaning a low value of k and a high value of l_0 . A value of 1 indicates that the cable should be "shrunk" with a high value of k and a low value of l_0 . Intermediate values indicate intermediate behavior.

Another feature of the cable controller is that it has a low pass (LP) filter between the command input and the impedance controller. This LP filter causes a slower cable reaction, which simulates the slow reaction of the caterpillar muscle. Figure 7.3 summarizes the characteristics of the cable controller.

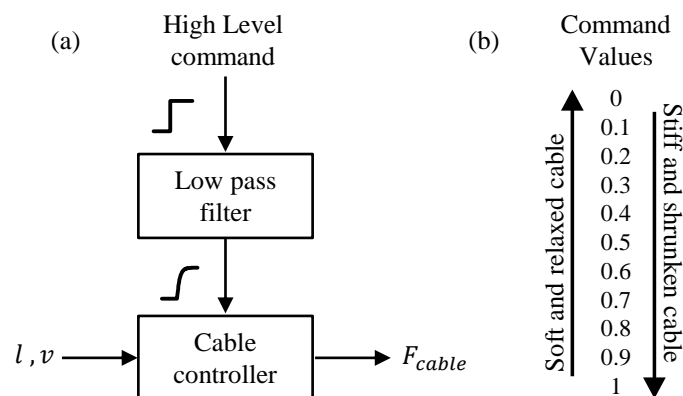


Figure 7.3: The cable controller. (a) The cable controller gets a high-level command which passes through a low pass (LP) filter. (b) The command receives values between 0 and 1, which controls cable behavior.

7.2.3 Legs

Legs have only two final positions: lifted or lowered. The state of the leg is determined by the high-level control, and the leg controller is responsible for the transition between these positions. This transition is controlled by a simple motion controller: the controller creates a cubic path between initial and final positions (there are only two paths: from lowered to lifted and from lifted to lowered).

The leg controller is also responsible for ground gripping. The algorithm for “locking” the leg to the ground is described in Figure 7.4. Note that when a leg is locked to the ground it cannot move, but it can still rotate (as in a pinned connection).

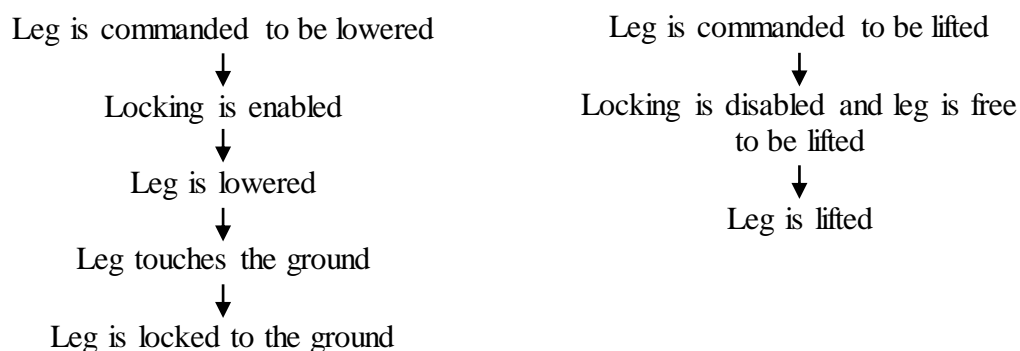


Figure 7.4: Leg locking algorithm.

Finally, the leg controller is responsible for sending a signal to the high-level control unit when the leg touches the ground.

7.3 High-Level Control

High-level control coordinates the movements of the caterpillar by controlling the cables and the legs of each segment. Cables are controlled using the ‘command’ inputs which receive values between 0 and 1. Legs are controlled using a binary input which triggers lifting or lowering of the leg. Therefore, for an eight segments caterpillar model, the high-level control needs to control 16 continuous parameters (for 16 cables, two cables in each segment) and 9 binary parameters (for 9 legs).

The nomenclature for the legs, segments and cables that will be used in the remainder of this chapter is shown in Figure 7.5. Note that all elements are numbered starting at the posterior side.

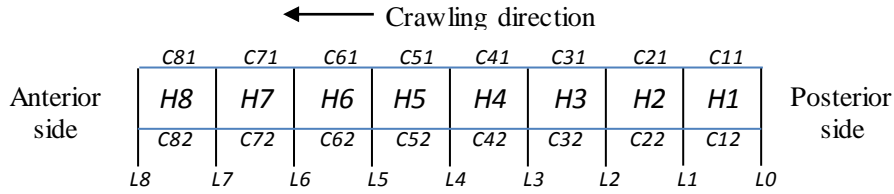


Figure 7.5: Numbering of the legs, cables and segments. L is used to denote a leg, C is used to denote a cable and H is used to denote a segment.

One crawling stride of the caterpillar is defined as a complete movement of a contraction wave from the posterior (back side) of the caterpillar to its anterior (front side). Each stride is divided into several steps as follows:

- step 1: The first step in a stride starts with the lifting of $L0$ and ends when $L0$ touches the ground.
- step 2: The second step starts when $L0$ touches the ground and ends when the $L1$ touches the ground.
- ⋮
- step 9: The last step starts when $L7$ touches the ground and ends when $L8$ touches the ground.

Figure 7.6 illustrates the different steps of a crawling stride. The snapshots in this figure show the starting position of each step.

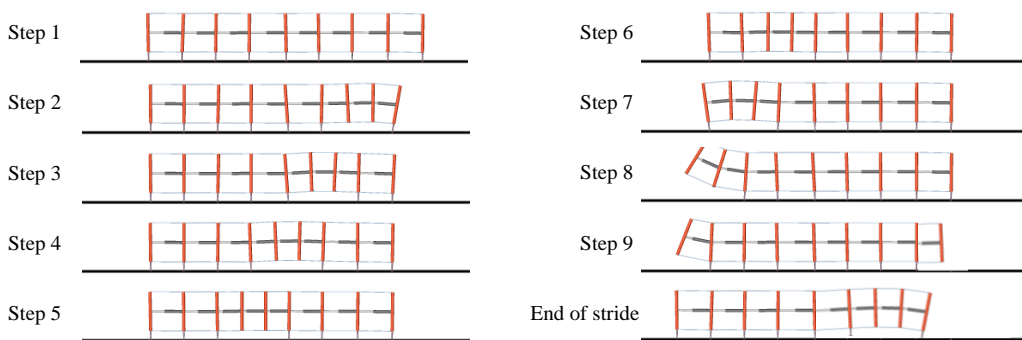


Figure 7.6: A complete stride of the caterpillar model is composed of 9 steps.

The high-level control algorithm has the following characteristics:

1. The transition from step to step is triggered by the contact of the legs with the ground.

2. In each step, up to three segments are in various stages of contraction and up to 3 legs are off the ground. This enables increased stride length.
3. A new stride starts before the previous stride ends. This enables increased stride frequency.

The two last characteristics can be seen in Figure 7.6.

High-level control is divided to 2 levels: level 1 and level 2. The following sections describe the infrastructure of these two levels.

7.3.1 Level 1 control

This level of control is equivalent to the Central Pattern Generator (CPG) of the caterpillar (See section 2.2) and is responsible for the coordination of the movements of the cables and legs. This level of control does not take into consideration the terrain shape and provides commands suitable only for flat terrain.

The level 1 control activates several segments at a time, depending on the present stride step. The other segments are in 'resting' state. In the first step the rear segments are activated, and as the stride proceeds, the activation of the segments moves forwards.

The activated time of each segment is called the *swing phase* and the resting time of a segment is called the *stance phase*. The swing phase of a segment starts when its posterior leg is lifted, and ends when its anterior leg is lowered.

In each step, level 1 control sends commands to the activated segments (cables and legs). The commands of each step are time dependent and change as the step proceeds.

For example, consider step 1:

In step 1, segments *H1-H3* are activated and start their swing phase. Figure 7.7 shows how the commands of each cable and leg change as a function of time. Remember that the step does not end after a particular time; rather, it ends when *L0* touches the ground. For example, if *L0* touches the ground after 0.2 s, the subsequent commands of step 1 will not be executed, and step 1 will cease to affect motion.

When step 1 ends, the three segments continue their swing phase (segment *H1* enters the stance phase only at the end of step 2) and remain activated under the control of step 2.

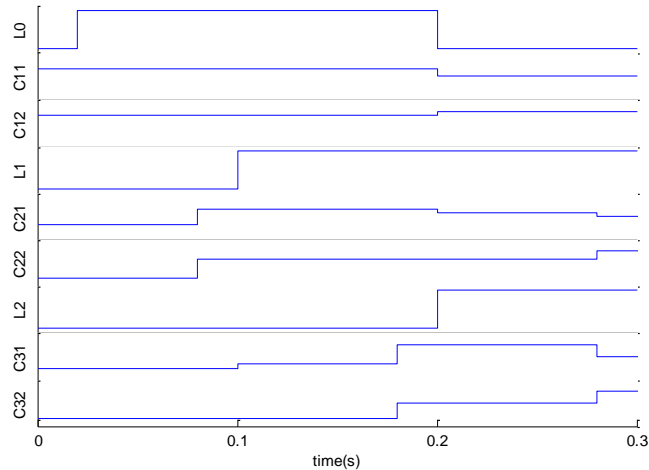


Figure 7.7: The commands sent to the cables and legs in step 1. Commands are delivered to the activated segments (*H1-H3*) and change during time.

Each step activates different sets of segments and issues a distinct set of commands. Each stride, however, issues the same set of step commands. The only thing that can change is the duration of the step, which can differ from stride to stride as it is dependent on ground contact.

7.3.2 Level 2 control

This level of control is local: each segment has its own control unit, equivalent to the ganglia spread over the biological caterpillar segments. Level 2 control is responsible for fitting motion to the terrain shape.

This control has two modes:

One mode for controlling segments in stance phase (when the segment is at rest and thus not controlled by level 1 control) and adjusting them to the terrain. A second mode for segments in swing phase (when the segment is activated and thus controlled by level 1 control). In the second mode, the level 2 control mediates between level 1 commands and the cable controllers, adjusting the commands to the terrain.

Mode I: Adjusting a segment in stance phase to the terrain shape

The algorithm is based on the assumption that when both legs of each side of a segment touch the ground, the segment has only 1 DOF – the bending angle (although the assumption is not completely accurate, see section 6.3.3). The bending angle is a function of cable length, which in turn is a function of the cable's command. A simple algorithm for calculating the cable's command for a desired bending angle is

described in Appendix B. This algorithm is referred to as the *single segment algorithm*.

The complete algorithm assumes that, for the model to perfectly fit the terrain, each segment bar (and the leg connected to it) must be exactly perpendicular to the terrain. Although the complete algorithm does not perfectly fulfill this criterion, it is relatively simple and adequate for our application.

Before describing the complete algorithm, consider the case of two segments with arbitrary bending angles of α and β . The algorithm for adjusting them to the terrain is as follows:

1. Find the average of the segment angles: $\frac{(\alpha+\beta)}{2}$.
2. Use the single segment algorithm for adjusting each segment to this angle.

Figure 7.8 shows an illustration of this algorithm. For clarity, only the bars (represented as rigid lines) and top cables (represented as dashed lines) are drawn. It can be seen that using this algorithm makes the segment bars (the rigid lines) nearly perpendicular to the terrain. This algorithm performs terrain adjustments well while maintaining simplicity and is referred to as the *two-segments algorithm*.

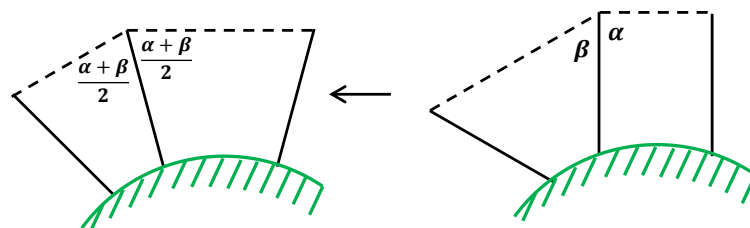


Figure 7.8: Illustration of the two-segments algorithm. By setting the bending angle of both segments to the average angle, the segment has a better fit to the terrain.

The complete algorithm uses the algorithms described above and works locally: each time a certain leg touches the ground, one of the algorithms - the single-segment or the two-segments - is performed on the segments posterior to that leg (and are in stance phase). In detail, the algorithm works as follows:

- When *LO* touches the ground nothing happens. The algorithm is not activated since segment *HI* is still not fully grounded and continues the swing phase.

- When $L1$ touches the ground, segment $H1$ enters the stance phase and the single-segment algorithm is performed on that segment. The segment's angle is set to a default value of 90° .
- When $L2$ touches the ground segment $H2$ enters the stance phase and the two-segments algorithm is performed on $H2$ & $H1$.
- The same is true for the remainder of the stride: each leg activates the two-segments algorithm for its two posterior segments.

Mode II: Adjusting a segment in swing phase to the terrain shape

A segment in swing phase is adjusted to the terrain by a combination of two sets of commands:

1. the commands arriving at the segment from level 1 control.
2. the stance phase commands of the segment, before it became activated (these commands are assumed to fit the terrain, as described above)

To describe how this combination is calculated, first the following two expressions are defined:

$$\begin{aligned} C1^* &= \tilde{C}1 + \frac{R1 - R2}{2} \\ C2^* &= \tilde{C}2 - \frac{R1 - R2}{2} \end{aligned} \quad (7.3)$$

where $\tilde{C}1, \tilde{C}2$ are the commands arriving from the level 1 control of the top and bottom cables respectively and $R1, R2$ are the stance phase commands of the top and bottom cables respectively.

The output commands of level 2 control to the cables – $C1, C2$ – are as follows:

$$\begin{aligned} C1 &= \begin{cases} 1 & \text{if } C1^* > 1 \\ C1^* & \text{if } 0 < C1^* < 1 \\ 0 & \text{if } C1^* < 0 \end{cases} \\ C2 &= \begin{cases} 1 & \text{if } C2^* > 1 \\ C2^* & \text{if } 0 < C2^* < 1 \\ 0 & \text{if } C2^* < 0 \end{cases} \end{aligned} \quad (7.4)$$

To understand the meaning of these equations, consider the example shown in Figure 7.9. The commands to the segment arriving from the level 1 control are $\tilde{C}1 = \tilde{C}2 = 0.7$, and tend to shrink the segments to a rectangular shape (since they are both equal). On the other hand, the resting segment bends to fit a convex terrain and have the

following commands: $R1 = 0$, $R2 = 0.4$. The output commands are: $Ci1 = 0.5$, $Ci2 = 0.9$. They shrink the segment but also keep the segment bent; therefore the segment maintains terrain shape. Note that the algorithm has upper and lower bounds of 1 and 0 respectively.

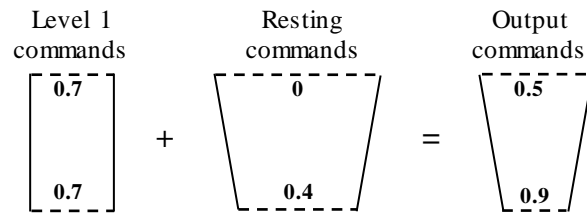


Figure 7.9: An example for calculating the output commands of level 2 control. The output commands are determined by a combination of level 1 commands and the resting commands.

8 Results

8.1 Model Characteristics

The biological descriptions of this chapter pertain to the *Manduca Sexta* species of caterpillar in its fifth instar (the last developmental stage before it becomes a pupa). In this stage the caterpillar weights about 2 g, and its dimensions are about 60 mm in length and 5mm in height [26].

When divided into 11 segments (3 thoracic + 8 abdominal, neglecting the small head), each segment weights about 0.18 g with an average length of around 5.5 mm.

While our model maintains consistency with the height and weight of the biological caterpillar, there is considerable discrepancy in segment length which will be discussed in 8.2.2.

8.2 Kinematic results

8.2.1 Crawling stages

In section 7.3 the different steps of the caterpillar crawl where shown in order to illustrate the algorithm which is used by the high-level control. Here, the strategy of the crawl is more deeply analyzed.

The complete stride is divided into three different stages. Illustration of these stages is shown in Figure 8.1, and the role of each stage is detailed below:

1. The role of the first stage is to initiate the crawl. In this stage, the rear part the caterpillar is lifted and shrunken. The stage ends when the posterior leg - $L0$ - is lowered and touches the ground (image 1d in Figure 8.1). The gap between the original position of $L0$ and its new position is the *stride length*. During this stage the lifted segments are supported only on one side.
2. The role of the second stage is to pass the wave through the body. In each step one segment is extended and relaxed and one segment is shrunken. For example, in the first step of the stage the posterior segment - $H0$ - is extended and $H4$ is shrunken (image 2a in Figure 8.1). Also, at each point in time there are 2-3 legs lifted. During this stage the lifted segments are supported on both sides.

3. The role of the third stage is to complete the stride. In this stage, the anterior leg - $L8$ - is lifted and the three anterior segments are kept shrunken in the air (image 3a in Figure 8.1). Then, the three segments are expanded one after the other. Similarly to stage 1, the lifted segments are supported on one side; yet, here the segments are extended, rather than compressed.

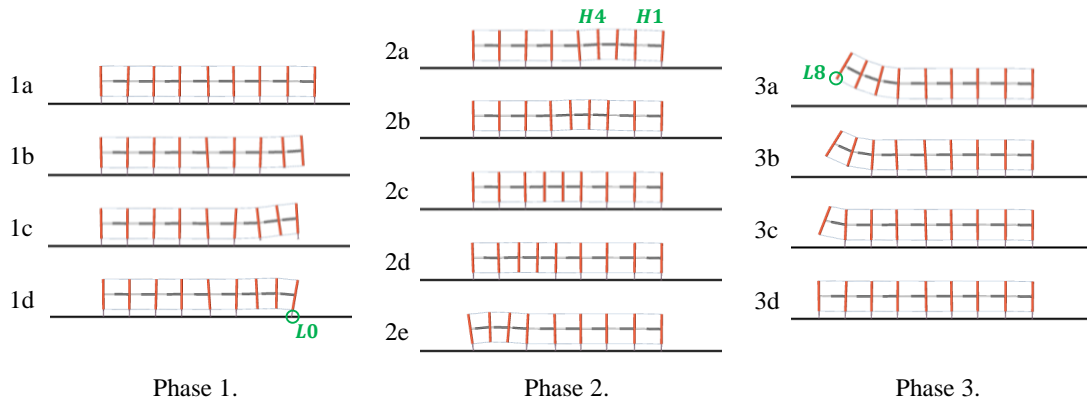


Figure 8.1: Crawl Stages.

In our model, the simulation is programmed such that the next stride begins when leg $L6$ touches the ground (when the crawl gets to the position shown in image 3b in Figure 8.1). For clarity, Figure 8.1 does not show the beginning of the next stride.

8.2.2 Segment length

The results given in the following sections for both the biological caterpillar and the caterpillar model were obtained from straight and horizontal crawling. Also, the caterpillar simulation reaches a steady state after 5 seconds of simulation. Therefore, the results shown here are the results that were obtained after this stabilization time.

The length of the struts (which is equivalent to the segment length) during crawling is shown in Figure 8.2 and Table 8.1.

Segment length changes by an average of 31%. This result is consistent with the observation of caterpillar muscles, which exhibit comparable shortening to 30% of resting length [9]. In contrast, the average stance (or resting) length of a segment is 4.45mm, which is significantly different from the approximate 5.54mm in the biological caterpillar. The average duty factor in our model is 46%. The biological caterpillar has a duty factor of 41%.

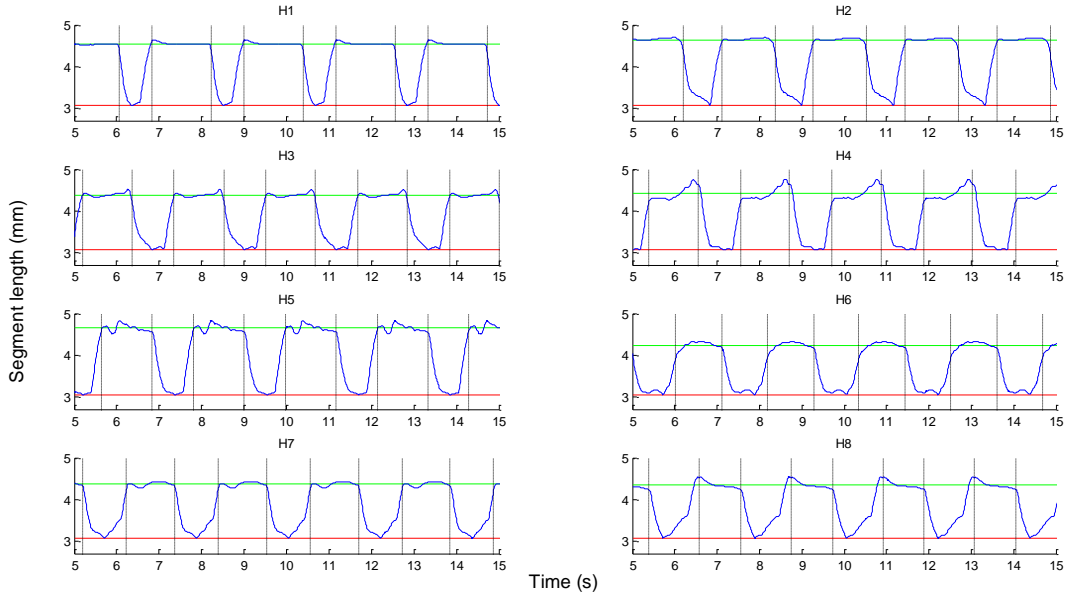


Figure 8.2: Strut length during crawling. The dashed line indicates transitions between swing and stance. The green line indicates average length in stance, and the red line indicates minimum length in swing.

Table 8.1: Strut length and step times during crawling.

Segment	Stance Length (mm)	Min length (mm)	Length change (%)	Stance time (s)	Swing time (s)	Step time (s)	Duty factor ¹² (%)
<i>H1</i>	4.55	3.07	32	1.40	0.76	2.16	35
<i>H2</i>	4.64	3.08	34	1.26	0.90	2.16	41
<i>H3</i>	4.38	3.06	30	1.17	0.99	2.16	46
<i>H4</i>	4.42	3.06	31	1.15	1.01	2.16	47
<i>H5</i>	4.65	3.05	34	1.20	0.96	2.16	44
<i>H6</i>	4.24	3.05	28	1.10	1.06	2.16	49
<i>H7</i>	4.36	3.06	30	1.14	1.02	2.16	47
<i>H8</i>	4.35	3.07	29	0.97	1.19	2.16	55
Average	4.45	3.06	31	1.17	0.99	2.16	46

8.2.3 Crawling parameters

In the biological caterpillar the average stride length is 8.52mm, and the average duration of one crawl is 2.78s [28]. Also, a new stride begins every 2.81s. The velocity of the biological caterpillar is 3.03 mm/s .

¹² Duty factor is the swing time as a fraction of the total time.

In the caterpillar model the stride length is 4.19mm, the duration of one stride is 2.71s and a new stride begins every 2.16s. The velocity of the caterpillar model is: $4.19mm \div 2.16s = 1.93 mm/s$.

The duration of one crawl is very similar (a difference of 2.5%) and shows that the dynamic behavior of the model is close to the behavior of the biological caterpillar (see also section 8.3). On the contrary, the stride length of the model is less than half that of the biological caterpillar. This is also reason for the big difference in the velocity.

Figure 8.3 shows the movement of the model's center of mass (C.M.) during crawling. It can be seen that during most of its motion the C.M. remains at a relatively constant height, except during stage 3. In this stage the three anterior segments are lifted and cause the C.M. to be raised.

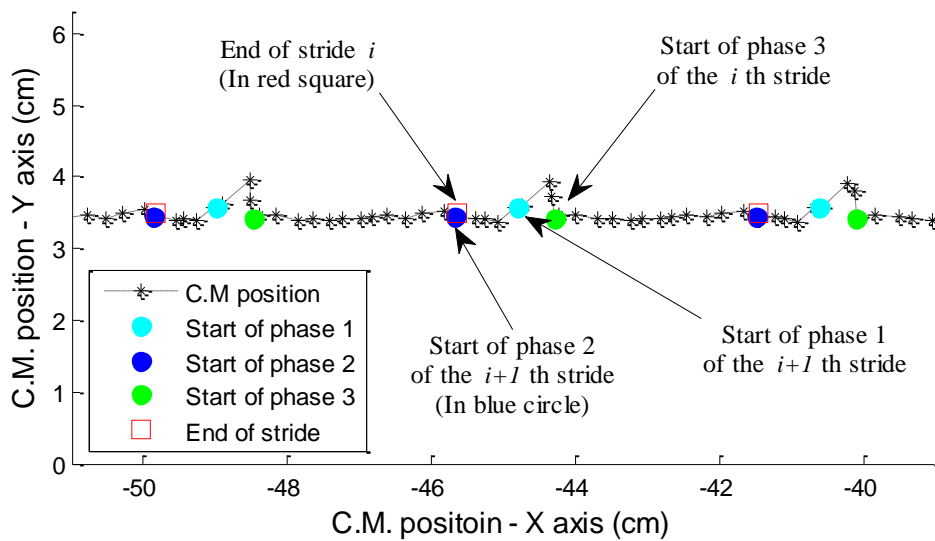


Figure 8.3: Movement of the center of mass (C.M.) during crawl. Time between two consecutive asterisks is 0.1s. Movement is from right to left.

8.3 Cable dynamics

Woods et al. [9] examined the behavior of a caterpillar muscle. In their paper they tested the course of force development by a caterpillar muscle under tetanic stimulus at resting length.¹³ To compare these results, a similar test was conducted on the

¹³ A tetanic stimulus is a strong and sustained stimulus.

model cable. Results are shown in Figure 8.4 and Table 8.1, which demonstrate that the behavior of the model cable is close to that of the caterpillar muscle, and both exhibit a similar time constant.

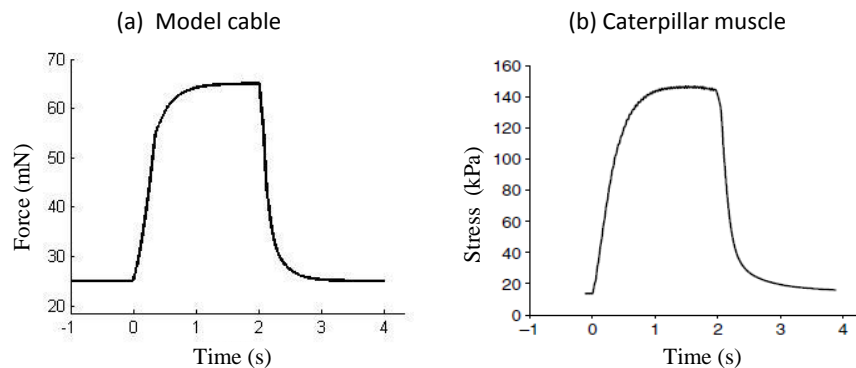


Figure 8.4: Force development under a tetanic stimulus of 2 seconds at resting length: (a) the model cable, and (b) the caterpillar muscle.

Table 8.2: Time of force development under a tetanic stimulus at resting length.

	Caterpillar muscle	Model cable
50% of peak force	0.27 s	0.26 s
80% of peak force	0.41 s	0.56 s

The change of cable forces in *H3* while crawling is shown in Figure 8.5. Other segments demonstrate similar behavior. The maximum change in cable forces is only 13.8% relative to resting force.

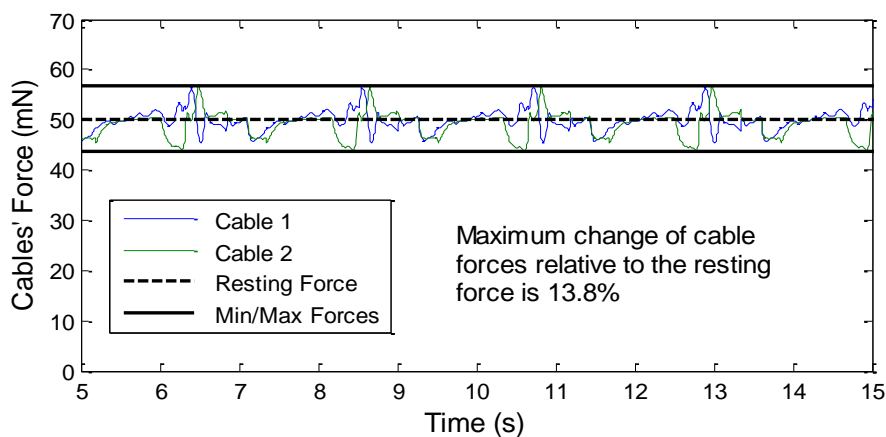


Figure 8.5: The change of cable force in *H3* while crawling in comparison to resting force.

8.4 Different terrains

The locomotion of the model was tested on various terrains. The following figures show snapshots of model locomotion on these terrains. The complete videos of can be found at <http://www.eng.tau.ac.il/~shai/studentlist.htm> .

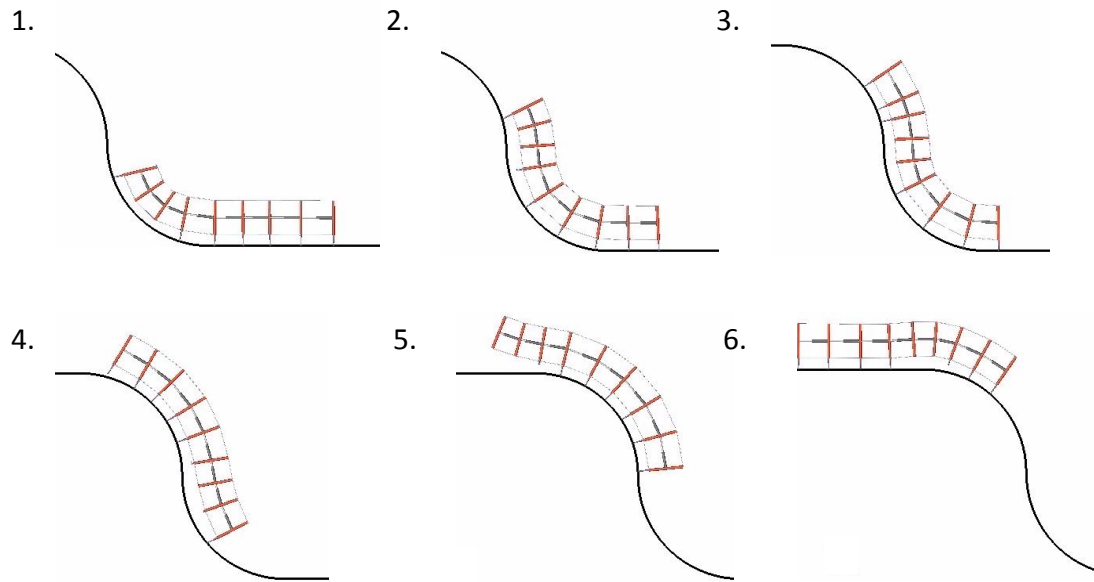


Figure 8.6: Model climb of sharp incline.

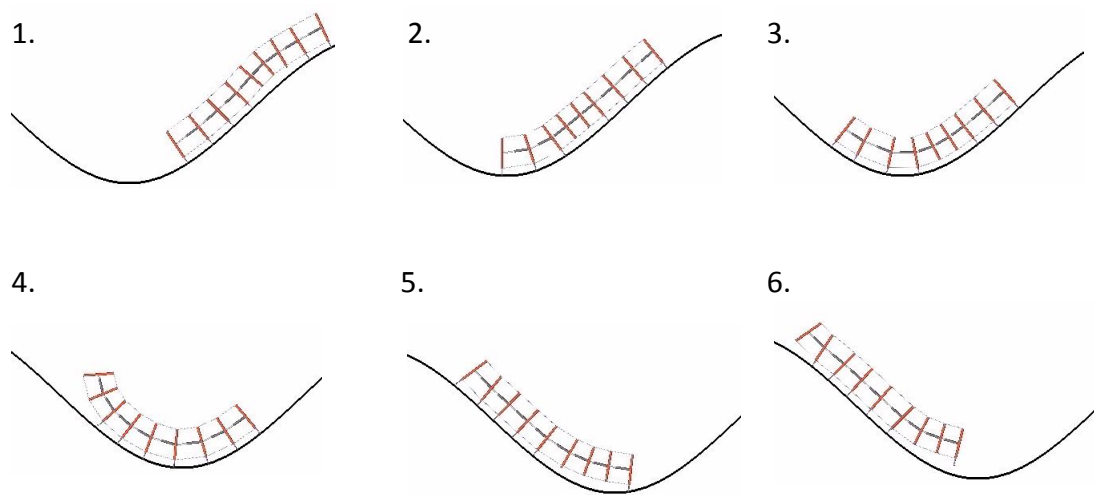


Figure 8.7: Model climb through curved terrain.

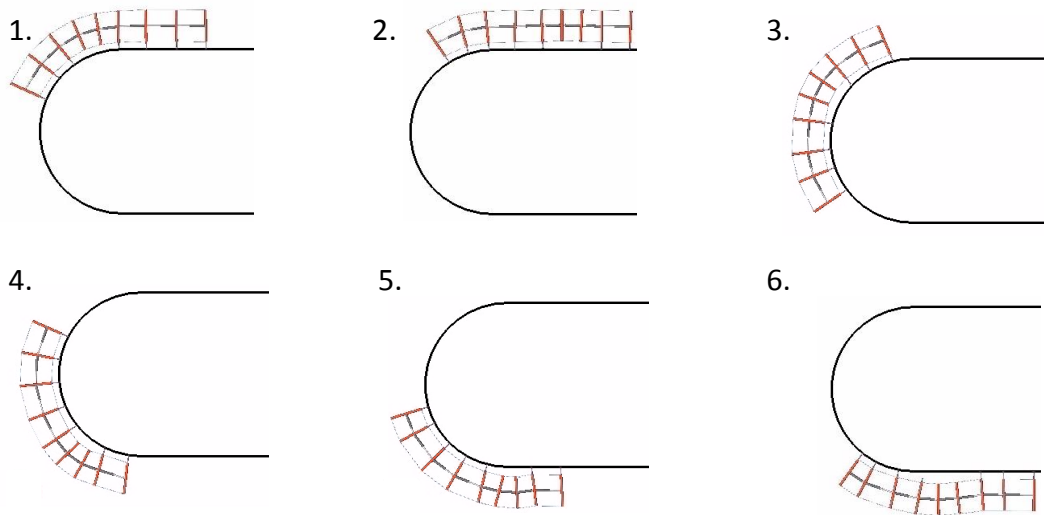


Figure 8.8: Model climbs upside down.

8.5 Other results

8.5.1 Area conservation

Caterpillar internal area while crawling is shown in Figure 8.9.

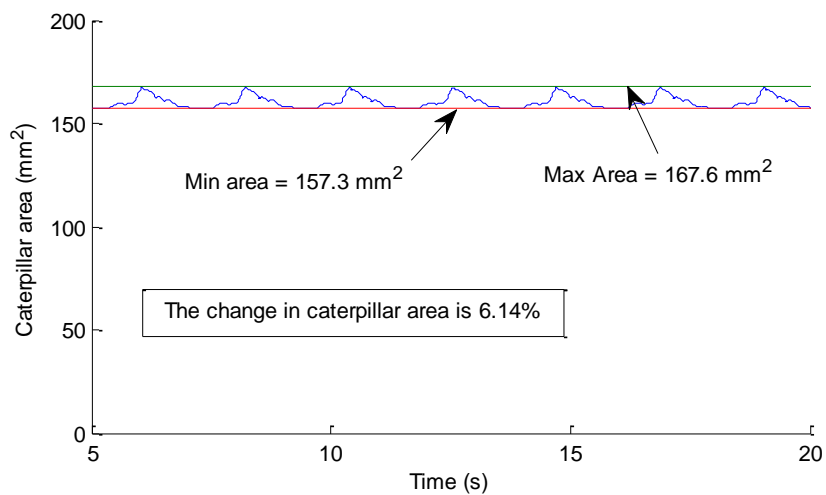


Figure 8.9: Change in caterpillar area during crawling.

The change in caterpillar area while crawling is only 6.14%. This result correlates with the observation that caterpillars have nearly constant volume (See section 6.2.3).

8.5.2 Internal Pressure

The model was tested with various levels of internal pressure - F_0 . As was shown in section 6.3.2, as long as F_0 is above a certain threshold, crawling is independent of the magnitude of internal pressure.

9 Discussion

The chapter will firstly discuss the use of impedance control for Assur tensegrity structures in general. Secondly, we will focus on the caterpillar model and what we can learn from it.

9.1 Controlling Assur tensegrity structures using impedance control

Impedance control is a well-known control scheme [24]. Nevertheless, no work has been done on its application to tensegrity structures.

We found that impedance control keeps the Assur tensegrity structure in singular configuration, thus maintaining the stability of the structure. In addition, impedance control enables us to produce a soft model with a controllable degree of softness.

The implementation of impedance control in our model is very simple since each element is controlled separately and independently. As mentioned in section 3.4, all tensegrity structures have infinitesimal motion at their singular configuration, and the actual passive compliance of the structure around this point is determined, among other things, by the elasticity of the materials. The passive compliance of a tensegrity structure is usually much greater than the passive compliance of a standard industrial robot. The use of impedance control in our model can be thought of as a way to increasing this compliance (where the stiffness coefficient k is equivalent to Young's modulus).

In addition, Assur tensegrity structures, unlike most other tensegrity structures, are statically determinate structures which allow simple shape change.

These two characteristics (simple control and passive compliance) make this combination (Assur tensegrity + impedance control) very useful for soft robotics. In contrast to using soft materials, this method requires relatively simple control; in contrast to using rigid bodies, it manifests softness. Figure 9.1.

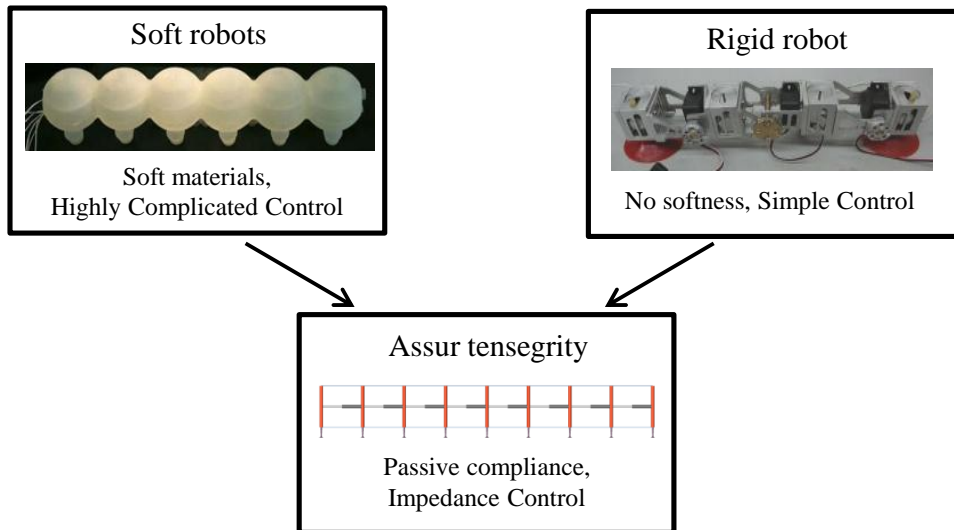


Figure 9.1: Comparing Assur tensegrity structures with other types of robots.

9.2 Caterpillar model

The model exhibits several characteristics which are analogous to those of the biological caterpillar as described in the following sections:

Empirical testing of the model has demonstrated that effective crawling requires that each stride be executed in three different stages, as described in section 8.2.1. Trimmer et al. [2] examined the kinematics of the biological caterpillar and found kinematic differences between three anatomic parts of the caterpillar: the thoracic segments, the midbody segments and the posterior segments. This distinction is similar to the three stride stages of the caterpillar model.

Also, caterpillar model can navigate different terrains and in different directions using the same crawling pattern without adjusting the control scheme. This is made possible by slow stride speed and firm ground planting. The same is true for the biological caterpillar [28].

The internal pressure of the biological caterpillar is not a function of its size. During growth, its body mass is increased 10,000-fold, while internal pressure remains constant [26]. In the same way, our model is able to use the same strut force regardless of model size.

It was proposed above that the mechanical properties of caterpillar muscles may assume responsibility for some of the control tasks otherwise carried out by the nervous system. Our model demonstrates that using impedance control for each cable

(which mimics the mechanical properties of caterpillar muscles) does indeed simplify high-level control. Also, caterpillar muscle develops force slowly. For comparison, caterpillar muscle force development is about four to seven times slower than that of an insect flight muscle [9]. The model show that adding the low pass filter to the cable controller, which makes the cable react slower, eases high-level control and results in smoother motion. Note that the time constant of the filter was determined empirically in order to optimize results. Only afterwards was the comparison made to the biological muscle, both of which exhibited similar time constants (Figure 8.4). In addition, other crawling parameters related to time (e.g., the duration of one stride) are comparable in both the model and the biological caterpillar.

On the other hand, there is a discrepancy between the stride length of the model and that of the biological caterpillar. There are two reasons for this discrepancy: Firstly, the biological caterpillar has longer segments. Secondly, the biological caterpillar can contract up to four segments at a time. In our model, only three segments are contracted at a time. The reason for this limitation is that, when four segments are contracted and lifted together, the impact of gravity becomes much larger (especially in stages 1 and 3, where segments are supported only on one side). This makes it difficult to program locomotion in a way that will be robust in all crawling directions (vertical and upside-down). This is also the reason that the all of the model segments have legs, in contrast to the biological caterpillar. Fixing this discrepancy requires the change of many control parameters and should be improved in future versions of the model.

Our research also suggests a few characteristics that the biological caterpillar may possess:

Cable forces do not change significantly during motion (Figure 8.5). They have more-or-less the same magnitude while crawling and while at rest. This suggests that caterpillars invest little additional energy when crawling as opposed to resting.

In our model, stride timing is strongly dependent on the signals that the legs send when touching the ground. Without those signals, locomotion is not robust – it tends to be inefficient and many times unstable. Observations show that feedback from the legs is not essential for maintaining locomotion gait in fast insects like the cockroach, while it is critical in slow insects like the *phasmid* (the stick insect) [29]. Although we

were not able to find similar information on the caterpillar, their slower gait makes it reasonable to assume that they also need leg feedback. The model introduced in this thesis strongly supports this hypothesis.

9.3 Further Research

Future research can follow three directions:

Firstly, the model can be improved in a number of ways. It should be optimized by increasing stride length. To do so, gravitational sensors would need to be added, which would allow for better control and better performance. In addition, the ability to control stride frequency would allow for variable velocity, and a more complex control algorithm could be designed to enable the model to navigate through obstacles and over gaps.

Secondly, the model can be expanded into three dimensions. The transition from two to three dimensions is possible but would present several complications, particularly because Assur trusses theory for three dimensional structures is not yet fully complete.

Finally, the construction of a physical mechanical model will greatly help to increase our understanding of these types of soft/rigid robots.

Bibliography

- [1] G. Chapman, "The hydrostatic skeleton in the invertebrates," *Biological reviews*, vol. 33, no. 3, pp. 338-371, August 1958.
- [2] B. Trimmer and J. Issberner, "Kinematics of soft-bodied, legged locomotion in *Manduca sexta* larvae," *The Biological Bulletin*, vol. 212, no. 2, pp. 130-142, April 2007.
- [3] B. A. Trimmer, A. E. Takesian and B. M. Sweet, "Caterpillar locomotion: A new model for soft-bodied climbing and burrowing robots," in *the 7th international symposium on technology and the mine problem*, 2006.
- [4] W. Wang, Y. Wang, W. K., H. Zhang and J. Zhang, "Analysis of the Kinematics of Module Climbing Caterpillar Robots," *Proceeding of 2008 IEEE/ASME International Conference on Advanced Intelligent Mechatronics*, pp. 84-89, 2008.
- [5] J. Stulce, "Conceptual design and simulation of a multibody passive-Legged crawling vehicle," Ph.D. dissertation, Virginia Polytechnic Institute and State University, Blacksburg, Virginia, 2002.
- [6] J. Rieffel, F. Saunder, S. Nadimpalli, H. Zhou, S. Hassoun, R. J. and B.A. Trimmer, "Evolving Soft Robotic Locomotion in PhysX," *Proceedings of the 11th Annual Conference Companion on Genetic and Evolutionary Computation Conference*, 2009.
- [7] J. A. Rieffel, F. J. Valero-Cuevas and H. Lipson, "Morphological communication: exploiting coupled dynamics in a complex mechanical structure to achieve locomotion," *Journal of the royal society interface*, vol. 7, no. 45, pp. 613-621, April 2010.
- [8] J. Eaton, *Lepidopteran Anatomy*, 1st ed., New York: John Wiley, 1988.
- [9] W. Woods, S. Fusillo and B.A. Trimmer, "Dynamic properties of a locomotory muscle of the tobacco hornworm *Manduca sexta* during strain cycling and simulated natural crawling," *Journal of Experimental Biology*, vol. 211, no. 6,

pp. 873-882, March 2008.

- [10] R. M. Johnston and R. B. Levine, "Crawling motor patterns induced by pilocarpine in isolated larval nerve cords of *Manduca sexta*," *Journal of neurophysiology*, vol. 76, no. 5, pp. 3178-3195, November 1996.
- [11] T. Casey, "Energetics of caterpillar locomotion: biomechanical constraints of a hydraulic skeleton," *Science*, vol. 252, no. 5002, pp. 112-114., April 1991.
- [12] R. B. Fuller, "Tensile-integrity structures". United States Patent 3,063,521, November 1962.
- [13] R. Motro, *Tensegrity: Structural Systems for the Future*, London: Kogan Page Science, 2003.
- [14] W. B. Whittier, "Kinematic Analysis of Tensegrity Structures," M.S thesis, Virginia Polytechnic Institute and State University, Blacksburg, Virginia, 2002.
- [15] C. Sultan and R. E. Skelton, "Deployment of tensegrity structures," *International Journal of Solids and Structures*, vol. 40, no. 18, p. 4637–4657, September 2003.
- [16] J. van de Wijdeven and B. de Jager, "Shape change of tensegrity structures: design and control," in *American Control Conference*, 2005.
- [17] D. E. Ingber, "The architecture of life," *Scientific American*, vol. 1, no. 278, January 1998.
- [18] L. Assur, "Issledovanie ploskih sterznevyyh mehanizmovs nizsimi paramis tocki zreniya ih struktury i klassifikacii," *Izdat. Akad. Nauk SSSR*, 1952.
- [19] I. I. Artobolevskii, *Teoriya mehanizmov i masin*, 2nd ed., Moscow-Leningrad: Gosudarstv. Izdat. Tehn.-Teor., 1951.
- [20] B. Servatius, O. Shai and W. Whiteley, "Geometric properties of Assur graphs," *European Journal of Combinatorics*, vol. 31, no. 4, pp. 1105-1120, May 2010.
- [21] O. Shai, "Topological Synthesis of All 2D Mechanisms through Assur Graphs," in *Proceedings of the ASME Design Engineering Technical Conferences*, 2010.
- [22] A. Bronfeld, "Shape change algorithm for a tensegrity device," M.S. thesis, Tel-Aviv University, Tel-Aviv, Israel, 2010.
- [23] J. J. Craig, *Introduction to robotics : mechanics and control*, 3rd ed., Upper Saddle River, New Jersey: Pearson Education, 2005.
- [24] N. Hogan, "Impedance control: An approach to manipulation. Parts I-III.,"

Journal of Dynamic Systems, Measurement, and Control, vol. 107, no. 1, pp. 1-24, March 1985.

- [25] H. T. Lin and B. A. Trimmer, "The substrate as a skeleton: ground reaction forces from a soft-bodied legged animal," *The Journal of Experimental Biology*, vol. 213, no. 7, pp. 1133-1142, April 2010.
- [26] H. T. Lin, D. J. Slate, C. R. Paetsch, A. L. Dorfmann and B. A. Trimmer, "Scaling of caterpillar body properties and its biomechanical implications for the use of hydrostatic skeleton," *The Journal of Experimental Biology*, vol. 214, no. 7, pp. 1194-1204., April 2011.
- [27] A. Dorfmann, B. Trimmer and W. Woods, "A constitutive model for muscle properties in a soft-bodied arthropod," *Journal of the Royal Society Interface*, vol. 4, no. 13, pp. 257-269, April 2007.
- [28] L. I. van Griethuijsen and B. A. Trimmer, "Kinematics of horizontal and vertical caterpillar crawling," *The Journal of Experimental Biology*, vol. 212, no. 10, pp. 1455-1462, May 2009.
- [29] E. Fuchs, P. Holmes, T. Kiemel and A. Ayali, "Intersegmental coordination of cockroach locomotion: adaptive control of centrally coupled pattern generator circuits," vol. 4, p. 125, January 2011.

Appendix A - Development of the equations for shape change and softness.

The following two sections present the development of equations (6.12) - (6.17). Section A.1 analyzes shape change without external forces, and section A.2 analyzes the effect of external forces (meaning softness). The lengths, forces, torques and reactions that a segment possesses and which will be used in our analysis are shown in Figure A.1.

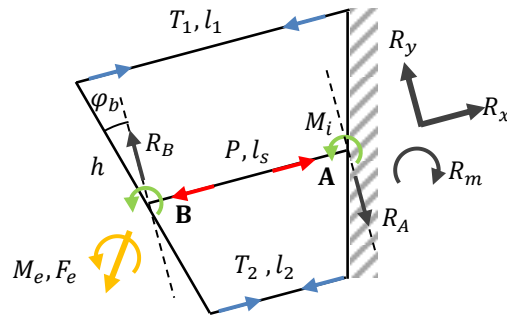


Figure A.1: Segment lengths, forces, torques and reactions.

A.1. Shape change without external forces

Since there are no external forces, reactions R_m, R_y, R_x equal zero. Equilibrium on each bar in y direction gives: $R_A = R_B = 0$. The other equilibrium equations are:

$$\begin{cases} \Sigma F_x : T_1 + T_2 - P = 0 \\ \Sigma M_A : T_1 \frac{h}{2} \cos \varphi_b - T_2 \frac{h}{2} \cos \varphi_b + M_i = 0 \\ \Sigma M_B : -T_1 \frac{h}{2} \cos \varphi_b + T_2 \frac{h}{2} \cos \varphi_b + M_i = 0 \end{cases}$$

Placing:

$$T_1 = \frac{F_0}{2} + k_1(l_1 - l_{0,1}), \quad T_2 = \frac{F_0}{2} + k_2(l_2 - l_{0,2}) \quad \text{and} \quad P = F_0$$

Gives:

$$\left\{ \begin{array}{l} \frac{F_0}{2} + k_1(l_1 - l_{0,1}) \frac{F_0}{2} + k_2(l_2 - l_{0,2}) - F_0 = 0 \\ \left(\frac{F_0}{2} + k_1(l_1 - l_{0,1}) \right) \frac{h}{2} \cos \varphi_b - \left(\frac{F_0}{2} + k_2(l_2 - l_{0,2}) \right) \frac{h}{2} \cos \varphi_b + M_i = 0 \\ - \left(\frac{F_0}{2} + k_1(l_1 - l_{0,1}) \right) \frac{h}{2} \cos \varphi_b + \left(\frac{F_0}{2} + k_2(l_2 - l_{0,2}) \right) \frac{h}{2} \cos \varphi_b + M_i = 0 \end{array} \right.$$

Adding eq. 2 to eq. 3 gives $M_i = 0$. The remaining two equations are:

$$\left\{ \begin{array}{l} \frac{F_0}{2} + k_1(l_1 - l_{0,1}) + \frac{F_0}{2} + k_2(l_2 - l_{0,2}) - F_0 = 0 \\ \left(\frac{F_0}{2} + k_1(l_1 - l_{0,1}) \right) \frac{h}{2} \cos \varphi_b - \left(\frac{F_0}{2} + k_2(l_2 - l_{0,2}) \right) \frac{h}{2} \cos \varphi_b = 0 \end{array} \right.$$

This can be reduced to:

$$\begin{cases} k_1(l_1 - l_{0,1}) = -k_2(l_2 - l_{0,2}) \\ k_1(l_1 - l_{0,1}) = k_2(l_2 - l_{0,2}) \end{cases}$$

The solution of these equations is:

$$l_1 = l_{0,1}, \quad l_2 = l_{0,2}$$

Strut length and shear angle can be calculated by:

$$l_s = \frac{1}{2}(l_1 + l_2) \quad \varphi_b = \sin^{-1} \left(\frac{l_1 - l_2}{2h} \right)$$

A.2. Softness

The analysis is performed only for the case that both cables have the same virtual force ($l_{0,1} = l_{0,2}$) and stiffness coefficient ($k_1 = k_2$), which will be denoted as l_o and k respectively. Also, analysis is performed for the three following cases: (a) axial force, (b) bending torque and (c) bending force.

A.2.1. Axial force

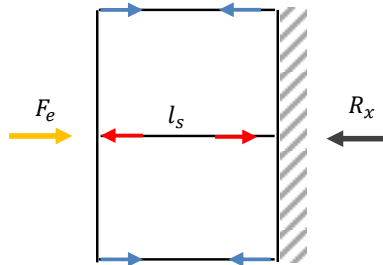


Figure A.2: A segment under axial force.

Equilibrium on the whole segment gives: $R_x = F_e$, $R_y = 0$, $M_e = 0$. Equilibrium on each bar in y direction gives: $R_A = R_B = 0$. The other equilibrium equations are:

$$\begin{cases} \Sigma F_x : F_e + T_1 + T_2 - P = 0 \\ \Sigma M_A : T_1 \frac{h}{2} - T_2 \frac{h}{2} + M_i = 0 \\ \Sigma M_B : -T_1 \frac{h}{2} + T_2 \frac{h}{2} + M_i = 0 \end{cases}$$

Again, adding eq. 2 to eq. 3 gives $M_i = 0$. Placing:

$$T_1 = \frac{F_0}{2} + k(l_1 - l_0), \quad T_2 = \frac{F_0}{2} + k(l_2 - l_0) \quad \text{and} \quad P = F_0$$

Gives:

$$\begin{cases} F_e + \frac{F_0}{2} + k(l_1 - l_0) + \frac{F_0}{2} + k(l_2 - l_0) - F_0 = 0 \\ \left(\frac{F_0}{2} + k(l_1 - l_0) \right) \frac{h}{2} - \left(\frac{F_0}{2} + k(l_2 - l_0) \right) \frac{h}{2} = 0 \end{cases}$$

This can be reduced to:

$$\begin{cases} l_1 + l_2 = 2l_0 - \frac{F_e}{k} \\ l_1 - l_2 = 0 \end{cases}$$

And the solution is:

$$l_1 = l_2 = l_0 - \frac{F_e}{2k} \rightarrow l_s = l_0 - \frac{F_e}{2k}, \quad \varphi_b = 0$$

Cable force must be greater than zero. Therefore:

$$\frac{F_0}{2} + k(l_1 - l_0) > 0 \rightarrow \frac{F_0}{2} + k\left(l_0 - \frac{F_e}{2k} - l_0\right) > 0 \rightarrow F_e < F_0$$

This means that the external force must be less than the strut force (F_0) in order to maintain segment stability. This is only for external compression force. There is no mathematical limit for tension force.

A.2.2. Bending torque

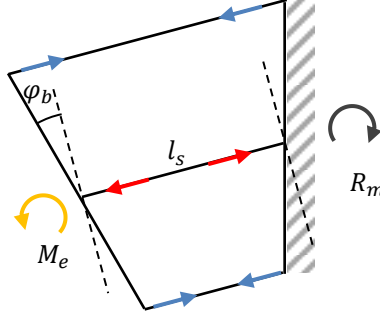


Figure A.3: A segment under bending torque.

Equilibrium on the whole segment gives: $R_x = R_y = 0$, $R_m = M_e$. Equilibrium on each bar in y direction gives: $R_A = R_B = 0$. The other equilibrium equations are:

$$\begin{cases} \Sigma F_x : T_1 + T_2 - P = 0 \\ \Sigma M_A : T_1 \frac{h}{2} \cos \varphi_b - T_2 \frac{h}{2} \cos \varphi_b + M_i - R_m = 0 \\ \Sigma M_B : -T_1 \frac{h}{2} \cos \varphi_b + T_2 \frac{h}{2} \cos \varphi_b + M_i + M_e = 0 \end{cases}$$

Adding eq. 2 to eq. 3 gives:

$$2M_i = R_m - M_e = 0 \rightarrow M_i = 0$$

Placing the expressions for T_1, T_2 and P in the remaining two equations gives:

$$\begin{cases} \frac{F_0}{2} + k(l_1 - l_0) + \frac{F_0}{2} + k(l_2 - l_0) - F_0 = 0 \\ -\left(\frac{F_0}{2} + k(l_1 - l_0)\right) \frac{h}{2} \cos \varphi_b + \left(\frac{F_0}{2} + k(l_2 - l_0)\right) \frac{h}{2} \cos \varphi_b + M_e = 0 \end{cases}$$

This can be reduced to:

$$\begin{cases} l_1 + l_2 = 2l_0 \\ l_1 - l_2 = \frac{2M_e}{kh \cos \varphi_b} \end{cases}$$

Therefore:

$$\begin{cases} l_s = \frac{1}{2}(l_1 + l_2) = l_0 \\ \sin \varphi_b = \frac{l_1 - l_2}{2h} = \frac{M_e}{kh^2 \cos \varphi_b} \end{cases}$$

For small angles, it can be approximated that $\cos \varphi_b \approx 1$ and $\sin \varphi_b \approx \varphi_b$ which simplifies the expression for the bending angle to:

$$\varphi_b \approx \frac{M_e}{kh^2}$$

Cable forces must be greater than zero. Therefore:

$$T_2 = \frac{F_0}{2} + k(l_2 - l_0) = \frac{F_0}{2} + k(l_s - h \sin \varphi_b - l_0) \approx \frac{F_0}{2} + k \left(l_0 - h \frac{M_e}{kh^2} - l_0 \right) > 0$$

$$\rightarrow M_e < \frac{F_0 h}{2}$$

Note that the limitation of the bending moment magnitude does not depend on its direction. For a positive moment the limitation is due to a decreasing tension of the bottom cable (T_2), and for a negative moment the limitation is due to a decreasing tension of the upper cable (T_1).

A.2.3. Bending force

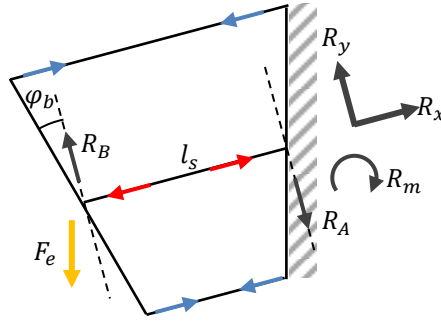


Figure A.4: A segment under bending force.

Equilibrium on the whole segment gives:

$$R_x = F_e \sin \varphi_b, \quad R_y = F_e \cos \varphi_b, \quad R_m = F_e l_s \cos(2\varphi_b)$$

Equilibrium on each bar in y direction gives:

$$R_A = R_B = F_e \cos \varphi_b$$

The other equilibrium equations are:

$$\begin{cases} \Sigma F_x : T_1 + T_2 - P - F_e \sin \varphi_b = 0 \\ \Sigma M_A : T_1 \frac{h}{2} \cos \varphi_b - T_2 \frac{h}{2} \cos \varphi_b + M_i - R_m = 0 \\ \Sigma M_B : -T_1 \frac{h}{2} \cos \varphi_b + T_2 \frac{h}{2} \cos \varphi_b + M_i = 0 \end{cases}$$

Adding eq. 2 to eq. 3 gives:

$$2M_i = R_m \rightarrow M_i = \frac{1}{2}F_e l_s \cos(2\varphi_b)$$

Placing the expressions for T_1, T_2 and P in the remaining two equations gives:

$$\begin{cases} \frac{F_0}{2} + k(l_1 - l_0) + \frac{F_0}{2} + k(l_2 - l_0) - F_0 - F_e \sin \varphi_b = 0 \\ \left(\frac{F_0}{2} + k(l_1 - l_0)\right)\frac{h}{2} \cos \varphi_b - \left(\frac{F_0}{2} + k(l_2 - l_0)\right)\frac{h}{2} \cos \varphi_b - \frac{1}{2}F_e l_s \cos(2\varphi_b) = 0 \end{cases}$$

This can be reduced to:

$$\begin{cases} l_1 + l_2 = 2l_0 + \frac{F_e \sin \varphi_b}{k} \\ l_1 - l_2 = \frac{F_e l_s \cos(2\varphi_b)}{kh \cos \varphi_b} \end{cases}$$

This equals:

$$\begin{cases} 2l_s = 2l_0 + \frac{F_e \sin \varphi_b}{k} \\ 2h \sin \varphi_b = \frac{F_e l_s \cos(2\varphi_b)}{kh \cos \varphi_b} \end{cases}$$

For small bending angles the approximate solution is:

$$\begin{cases} l_s \approx l_0 \\ \varphi_b \approx \frac{F_e l_0}{2kh^2} \end{cases}$$

Cables forces must be greater than zero:

$$\begin{aligned} T_2 = \frac{F_0}{2} + k(l_2 - l_0) = \frac{F_0}{2} + k(l_s - h \sin \varphi_b - l_0) \approx \frac{F_0}{2} + k\left(l_0 - h \frac{F_e l_0}{2kh^2} - l_0\right) > 0 \\ \rightarrow F_e < \frac{F_0 h}{l_0} \end{aligned}$$

Again, the limitation of the bending force magnitude does not depend on its direction.

Appendix B - Single-segment algorithm

The purpose of the algorithm is to change the shape of a grounded segment while keeping the ground reactions and internal torque as low as possible.

When both legs of a segment are connected to the ground, the segment has one DOF – the bending angle (see Figure 6.16). The forces that act on each bar of the segment are:

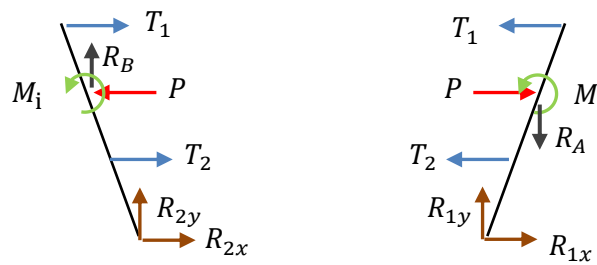


Figure B.1: The forces acting on each bar of a grounded segment.

In equilibrium the strut force equals F_0 . In the case that there is no gravity, it is easy to show that:

$$T_1 = T_2 = \frac{F_0}{2} \quad \rightarrow \quad M_i = 0, R_A = R_B = R_{1x} = R_{1y} = R_{2x} = R_{2y} = 0$$

The geometric parameters of the segment are:

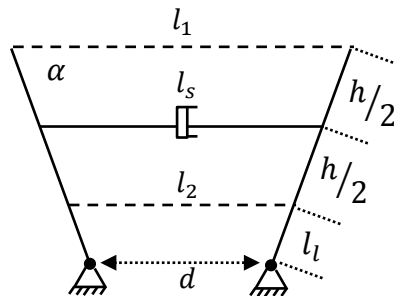


Figure B.2: The geometric parameters of the segment.

Where α is the segment angle, l_1 and l_2 are the cable lengths, l_s is the strut length, h is the bar length, l_1 is the leg length and d is the distance between two legs.

The calculation of d is given by:

$$d = l_s - \left(l_l + \frac{h}{2} \right) \cos \alpha$$

The needed lengths of the cables for a new segment angle α^* can be calculated by:

$$l_1^* = d + (l_l + h) \cos \alpha^* , \quad l_2^* = d + l_l \cos \alpha^*$$

Therefore, to change the shape of the segment from an angle α to a new angle α^* , while keeping the internal moment and ground reactions zero, the following algorithm is used:

1. Use the current l_s and α to calculate d .
2. Use d and the new angle α^* to calculate the new l_1^* and l_2^* .
3. Set the cable commands such that $T_1(l_1^*) = T_2(l_2^*) = \frac{F_0}{2}$

תקציר

הזחלים הינם בעלי חיים בעלי גוף רך, המשתמשים בנוזלים ובלחץ על מנת להקשיח את גופם, מכניזם הידוע כשלד הידרוסטאטי. לזחלים מערכת עצבים פשוטה יחסית, אך עדיין הם מסוגלים לבצע מגוון רחב של תנועות מורכבות.

עבודה זו מציגה סימולציה דו-מימדית של זחל, המחכה את תנועת הזחל על-ידי שימוש במבנים הנקראים "אסור טנזגריטי". מבני טנזגריטי הינם מבנים המורכבים מרשת לא רציפה של אלמנטים בלחיצה בתוך רשת רציפה של אלמנטים במתיחה. יציבותם של מבנים אלו נגרמת כתוצאה משיווי משקל פנימי של כלל האלמנטים. מבני "אסור טנזגריטי" הינם תת-קבוצה חדשנית של מבני טנזגריטי.

כל חוליה של הזחל, מיוצגת במודל כ"טריאדה" דו-מימדית המורכבת משני מוטות המחברים בעזרת שני כבלים ובוכנה. שני הכבלים מייצגים את שני השרירים האורכיים הראשיים של הזחל, בעוד הבוכנה מייצגת את השלד ההידרוסטאטי. בנוסף למבנה המכאני, גם סכמת הבקרה של המודל מבוססת על עקרונות הלקוחים מהזחל הביולוגי.

התכונות המיוחדות של מבני "אסור טנזגריטי", ביחד עם סכמת הבקרה המוצעת, יוצרים מודל הניתן לבקרה בצורה פשוטה ואינטואיטיבית. בנוסף, לחוליות במודל ישנה רמת רכות הניתנת לוויסות - כל חוליה יכולה להיות רכה או קשיחה.

בנוסף, למודל מספר תכונות הדומות לאלו של הזחל הביולוגי. דוגמא לתכונה שכזו, היא העובדה שהלחץ הפנימי של הזחל הביולוגי אינו תלוי בגודלו. במהלך גדילת הזחל, מסתו גדלה פי 10,000 בעוד הלחץ הפנימי נשאר קבוע. בדומה לכך, המודל יכול להשתמש באותם כוחות פנימיים, ללא תלות בגודל המודל. המודל שלנו גם מצביע על כך שזחלים אינם משקיעים אנרגיה רבה כאשר הם נעים, מעבר לאנרגיה אותה הם משקיעים במנוחה.

אוניברסיטת תל - אביב

הפקולטה להנדסה ע"ש איבי ואלדר פליישמן
בית הספר לתארים מתקדמים ע"ש זנדמן-סליינר

מודל עבור תנועת הזחל המבוסס על מבני אסור טנזגריטי

חיבור זה הוגש כעבודת גמר לקראת התואר "מוסמך אוניברסיטה" בהנדסה מכנית

על ידי

עומר עורקי

העבודה נעשתה בבית הספר להנדסה מכנית בהנחית

פרופ' עופר שי

ודר' אורי בן-חנן

אייר תשע"ב

אוניברסיטת תל - אביב

הפקולטה להנדסה ע"ש איבי ואלדר פלישמן
בית הספר לתארים מתקדמים ע"ש זנדמן-סליינר

מודל עבור תנועת הזחל המבוסס על מבני אסור טנזגריטי

חיבור זה הוגש כעבודת גמר לקראת התואר "מוסמך אוניברסיטה" בהנדסה מכנית

על ידי

עומר עורקי

אייר תשע"ב